Modifying and Measuring the Stiffness of a Regenerative Cardiac Scaffold *In Vitro*

Daniel Vincent Filipe

A thesis to be submitted to the faculty of Worcester Polytechnic Institute in partial fulfillment of the requirements for the Degree of Master of Science

Submitted by:

Daniel Filipe
Department of Biomedical Engineering

_____

Approved by:

Glenn Gaudette, PhD, Advisor
Associate Professor
Department of Biomedical Engineering

_____

Kristen Billiar, PhD
Associate Professor
Department of Biomedical Engineering

_____

Marsha Rolle, PhD
Assistant Professor
Department of Biomedical Engineering

_____

September 1, 2011

Acknowledgements

The length of time over which this project has extended has led me to be indebted to many people. I am particularly grateful to the following people without whom I could not have completed this project:

Jacques Guyette	Jason Hu
Megan Murphy	Jeffery John
Jeremy Skorinko	Jenna Balestrini
Jen Sansom	Tracy Gwyther
Evans Burford	Katie Bush
Jen Makridakis	Erin Heyer

I am grateful to Tim Butler (Genzyme Corporation) and my coworkers at Connective Orthopaedics for their understanding and encouragement as I split my time between working for them and completing this project.

The guidance of my advisors, particularly Glenn Gaudette, had made this project an invaluable educational experience.

Without the encouragement and unwavering patience of my wife Erika I would never have been able to complete this project.

Lastly, I could never have completed this project without the support of God, my family, and my friends.

Abstract

The stiffness of scaffolds used in surgical ventricular restoration may play an important role in the degree to which they facilitate regeneration of functional cardiac tissue. The stiffness of the scaffold influences the phenotype of cells which are present in it as well as their ability to deform the scaffold. The goal of this study was to evaluate *in vitro* methods to characterize and alter the stiffness of new scaffold materials.

Membrane inflation testing, an *in vitro* mechanical testing method, was evaluated in this study because of its ease of use and the similar mode of loading which it shares with scaffolds implanted *in vivo*. The structural stiffness of two scaffold materials, urinary bladder matrix and Dacron, were determined *in vivo* and using membrane inflation testing. Despite higher tensions and lower area stretch ratios for scaffolds tested using membrane testing, similar changes in structural stiffness between the two materials were found for both methods (5.6 ± 3.3 fold *in vivo*, 5.0 ± 1.0 *in vitro*). This finding demonstrated that membrane inflation testing is a useful *in vitro* method for measuring changes in structural stiffness between scaffold materials with a level of sensitivity similar to that which is measured *in vivo*.

Membrane inflation testing was used to assess the effectiveness of altering scaffold stiffness through exposure to various cell culture conditions. Incubation of a biological membrane in cell culture media resulted in a drastic decrease in the elastic modulus from its initial value (3.55 ± 0.52 MPa) after 2 weeks (1.79 ± 0.30 MPa), 4 weeks (1.04 ± 0.09 MPa), and 10 weeks (0.014 ± 0.01 MPa). When fibroblasts were cultured on the scaffolds for 10 weeks an increase in elastic modulus (0.134 ± 0.05 MPa) over scaffolds incubated in culture media for the same amount of time was observed. The increase in elastic modulus due to the presence of fibroblasts was accompanied by an increase in the percentage of collagen in the samples (54.1 ± 5.1 % without fibroblasts, 83.2 ± 5.1 % with fibroblasts). Contrary to expectation, addition of ascorbic acid to the media to increase production of collagen by the fibroblasts resulted in a decrease in elastic modulus (0.030 ± 0.01 MPa) compared to scaffolds cultured with fibroblasts in standard media and a decrease in the amount of enzymatically degraded collagen (40.8 ± 4.7 % without ascorbic acid, 21.1 ± 3.3 % with ascorbic acid).

Regeneration of cardiac tissue after a myocardial infarction is a complicated process which is influenced by a myriad of different factors. Future studies investigating the exact role which substrate stiffness has on regeneration will be essential to the development of improved cardiac scaffolds. Characterization of the stiffness of these scaffolds by membrane inflation and manipulation through exposure to cell culture conditions are powerful approaches to facilitate future studies.

Table of Contents

Table of Figures

Table of Tables

Chapter 1: Introduction

The primary function of the heart is to pump deoxygenated blood to the lungs and to pump oxygenated blood throughout the body. This function is accomplished as the chambers of the heart fill with blood and subsequently pressurize the blood to expel it out of the heart. This process is divided into two phases: systole, in which the heart muscle contracts to pressurize the blood, and diastole, in which the heart muscle relaxes to its resting state.

Congestive heart failure is a pathological condition which most frequently results from the development of scar tissue in the heart muscle. The increased stiffness of scar tissue reduces the ability of the heart muscle to contract and expel blood. The scar tissue can lead to irreversible stretch of remote un-scarred muscle, thus increasing the total volume of the heart. The increased stiffness and volume reduce the heart's ability to pump oxygenated blood throughout the body, thus decreasing the quality of life for affected patients (American Heart Association, 2008).

Many pharmacological interventions are used in the treatment of congestive heart failure. While these treatments may be effective in slowing scar formation, they are unable to reverse scarring once it has occurred (Gaudette & Cohen, 2006). In the case of extensive scarring both the negative effect on quality of life due to the reduced cardiac output and the danger of aneurysm may necessitate surgical intervention. Surgical intervention may come in the form of implantation of a synthetic polymer scaffold which is used to replace the aneurysm and alter the geometry of the vessel. Typical scaffolds serve to replace the weakened scar with a strong material and to reshape the geometry of the vessel so that it can pump blood more efficiently. Once implanted into the heart muscle, scaffolds are passively loaded during diastole as the muscle relaxes and the chamber expands while filling with blood. During systole, the scaffolds are unable to contribute to cardiac output for which active contraction of the heart wall is required. Recent research suggests that novel regenerative scaffold materials which foster the growth of new heart tissue may be able to restore the contractility of the infarcted region of the heart (Kelly, Rosen, Schuldt, Kochupura, Doronin, & Potapova, 2009) (Badylak, Kochupura, Cohen, Doronin, Saltman, & Gilbert, 2006). Although the initial behavior of these novel scaffolds is the same as that of typical scaffolds, the regeneration which occurs in these materials results in contribution to systole after substantial recovery has occurred.

Regenerative scaffolds are typically made from xenogeneic biological membranes. The stiffness of these scaffolds is thus dependent on the composition of the source tissue as well as the processing which it undergoes in order to remove cells and sterilize the material. Recent work with a variety of biological membrane scaffolds has demonstrated that when cells are seeded on these materials their stiffness is altered as the cells secrete extracellular matrix proteins and enzymes (Androjna, Spragg, & Derwin, 2007) (Long, Nagatomia, Chancellor, & Sacks, 2006) (Gentleman, Lay, Dickerson, & Nauman, 2003). Based on these results it was hypothesized that exposure of regenerative cardiac scaffolds to cell culture conditions would enable control of scaffold stiffness. The ability to alter scaffold stiffness *in vitro* has potential to pave the way for future studies investigating the range of scaffold stiffnesses which is optimal for regeneration.

The important role which scaffold stiffness plays in regeneration is primarily due to its influence on the phenotype of cells which make their way onto the scaffold as well as the impact which it has on the ability of the cells to eventually deform the scaffold. The stiffness of the substrate on which cells are grown has been well established as an important factor directing the differentiation pathway of progenitor cells (Discher, Janmey, & Wang, 2005) (Engler, Sen, Sweeney, & Discher, 2006). In addition, the stiffness of the scaffold cannot be too high or too low or the deformation will not match that of the surrounding heart tissue. If the stiffness of a scaffold is too high, it will not deform substantially and may impede diastolic filling, while if it is too low, it will undergo significant deformation and may balloon during diastole. The ability to characterize the stiffness of the scaffold is thus an important tool in the development of improved regenerative cardiac scaffolds.

Many *in vitro* methods are available to test the stiffness of scaffolds, each of which applies loads to the sample in a distinct manner, resulting in stiffness values which are unique to the particular mode of loading. Membrane inflation testing was evaluated in this study because of its ease of use and because it applies loads to scaffolds in a similar manner to that which occurs when they are implanted into the heart wall. Due to the similarities in the loading and deformation conditions which exist for scaffolds implanted *in vivo* and tested by membrane inflation, it was hypothesized that the structural stiffness of scaffolds tested using each of the methods would also be similar. An *in vitro* test method that yields stiffnesses which are similar to those which would exist *in vivo* would enable rapid and cost-effective comparisons to be made between candidate materials during development.

Future development of regenerative cardiac scaffolds will involve optimization of a number of characteristics ranging from the biochemical composition of the material to its biocompatibility. The findings of this study pave the way for future work to optimize one particular aspect of the scaffold – its stiffness, which can be altered by exposure to cell culture conditions and characterized using membrane inflation testing.

Chapter 2: Background

2.1 Congestive Heart Failure is a Result of Pathological Conditions and Geometric Remodeling

Heart Failure occurs when the ability of the heart to pump blood throughout the body drops to critically low levels. Situations like this arise from pathological conditions which negatively affect the structure or viability of cardiac tissue. These pathological conditions can be classified as ischemic conditions in which blood supply to the cardiac tissue is compromised, or as non-ischemic conditions in which the volume of the heart is enlarged as a result of a pre-existing condition. Acute ischemic disease caused by an extended blockage of the coronary artery may result in formation of a large scar within several weeks. Ischemic disease may also be chronic in which blockage of the coronary artery persists for a prolonged period of time. In this case many small areas of scarring may develop throughout the heart wall. Non-ischemic disease may develop as a result of valve insufficiencies, inflammatory conditions, or idiopathic causes (Tønnessen & Knudsen, 2005). All of these pathologies lead to the formation of regions of dead tissue called myocardial infarctions (MI). Severe MI's can develop into aneurysms in which the heart wall thins to the point at which it bursts. Aneurysms account for 23% of all deaths due to myocardial infarction (Zoffoli, Manino, Venturini, Terrini, Asta, & Zanchettin, 2009).

Dilation of the heart is a symptom that persists among all pathological conditions linked to chronic heart failure. In ischemic heart disease this dilation results from increasing stretch of viable heart tissue as it attempts to compensate for the akinetic scar regions. Even if reperfusion is used to treat the ischemic condition this stretch is often irreversible. The large scars present in acute conditions may also weaken as they thin out over time, eventually resulting in an aneurysm. This scarring also often leads to arrhythmias (Cox, 2004). Dilation of the ventricle is also characteristic in valve disease as the valve is unable to prevent the return of ejected blood back into the ventricle, resulting in a higher end-systolic volume and thus a greater overall volume. A similar response is seen in inflammatory conditions such as myocarditis.

Although dilation is a secondary result of a primary disease state, it is ultimately responsible for the life threatening failures which may occur. Cardiac dilation results in increased wall stress during diastole due to the higher radius of curvature. During systole there is an increase in energy and oxygen consumption as the sarcomeres stretch more in order to generate the higher force required to counteract this increased stress. High end systolic volume is directly related to reduced ejection fraction (Bax, et al., 2004). In addition, the increased end-diastolic volume which accompanies dilation has also been shown to be a primary clinical predictor of patient morbidity (Di Donato, Castelvecchio, & Menicanti, 2010) (Buckberg & Athanasuleas, 2009).

Enlargement of the heart also occurs with a shift in cardiac geometry from an elliptical to a spherical shape. It has been well documented in the literature that the unique fiber orientation which occurs in a healthy heart is essential to efficient cardiac function and that this orientation is lost during the transition to a spherical geometry (Sallin, 1969).

Standard treatments for congestive heart failure and the resulting dilation of the heart include medicinal treatments and revascularization using coronary artery bypass grafting (CABG). Many of the medications commonly prescribed to patients work by altering the physiology of the heart or of the blood vessels so that the blood can be pumped throughout the body more efficiently. Similarly, CABG is used to alter the anatomy of the heart's blood supply system and thus increase the amount of oxygen which the tissue receives. However, these methods are insufficient in cases in which scarring and stretch of muscle fibers has already occurred. Even if viable tissue is maintained through CABG, patients with severely dilated left ventricles do not experience a reduction in end systolic volume and thus continue to suffer from a reduced ejection fraction (Bax, et al., 2004).

2.2 Surgical Ventricular Restoration Reverses Geometric Remodeling

Surgical intervention is a promising treatment for patients in danger of an aneurysm or whose failing cardiac function has sufficiently compromised their quality of life (American Heart Association, 2008) (European Society of Cardiology, 2008). Surgical ventricular restoration (SVR) has evolved significantly over the last 50 years. The first type of procedure to be widely performed was resection of the aneurysm followed by linear closure of the adjacent tissue (Cooley, Collins, Morris, & Chapman, 1958) (Lillehei, Levy, Dewall, & Warden, 1962).

Dr. Randas Batista (Batista, et al., 1997) adapted this procedure for cases in which heart volume had increased due to non-ischemic conditions for which no large scar region existed. In this case a wedge of heart tissue from the apex to the papillary muscle was removed and the adjacent tissue was sutured together. This procedure has been largely abandoned due to high mortality rates (McCarthy, McCarthy, Starling, Smedira, Scalia, & Wong, 1998). This may be due to the fact that most non-ischemic and idiopathic forms of heart disease affect the heart in a non-homogeneous manner. Resection of a small portion is therefore only likely to do temporary good (Suma, Horii, Isomura, Buckberg, & Group, 2006).

The "Dor Procedure" was developed by Dr. Vincent Dor who replaced the scarred region with a scaffold (Kaza, et al., 2002) (Coskun, Popov, Coskun, Hinz, Schmitto, & Körfer, 2009). The ability to tailor the size of the scaffold allows the surgeon to have greater control over the post-operative volume of the heart. Patients undergoing the Dor procedure have a substantially higher cumulative survival compared to patients who undergo resection of the aneurysm alone (Lundblad, Abdelnoor, & Svennevig, 2004).

While the Dor procedure was a clear improvement over resection of the aneurysm followed by direct closure in that it corrected the increased size which occurred due to cardiac dilation, the post-operative ventricle was still spherical rather than conical in shape. The Surgical Anterior Ventricular Endocardial Restoration (SAVER) procedure was developed to restore the ventricle to its natural conical shape while excluding the scarred region using a scaffold (Suma, Horii, Isomura, Buckberg, & Group, 2006). Rather than placing a scaffold only over the scarred region it is placed along the endocardial wall between the apex of the ventricle and the septum. The placement of the scaffold in this procedure is also advantageous because it can be used to exclude scars which frequently occur in the septum. Retrospective studies have shown excellent results for large numbers of patients undergoing the SAVER procedure (Athanasuleas, Buckberg, Stanley, Siler, Dor, & Di Donato, 2004) (Di Donato, Castelvecchio, & Menicanti, 2010).

Despite the positive outcomes observed for SVR procedures, wide acceptance by the medical community has not been achieved in part due to the fact that many insurance companies consider them to be experimental and investigational procedures for which efficacy has not been established (Aetna, 2009) (Cigna, 2010). In particular the insurance companies cite the lack of randomized controlled clinical studies designed to compare the efficacy of SVR procedures to other currently used therapies. The importance of strong clinical evidence is highlighted by considering the economic impact of SVR. Mark et al. examined the total hospitalization costs of CABG vs. CABG combined with SVR and found that SVR added $14,500 to a procedure that already cost over $44,000 (Mark, Knight, Velazquez, Howlett, Spertus, & Djokovic, 2009). This increased cost comes primarily from longer procedure and recovery times. The Surgical Treatment for Ischemic Heart Failure (STICH) trial was designed to meet the need for a randomized controlled clinical trial. This study compared patients receiving only coronary artery bypass grafting (CABG) to those receiving CABG combined with SVR. The study concluded that although SVR reduced ventricular volume it did not improve symptoms over treatment with CABG alone. These conclusions were hotly contested however, due to substantial deviations from the proposed protocol and poor execution (Buckberg & Athanasuleas, 2009). Further studies are thus needed in order to provide clear evidence of the efficacy of SVR as insurance companies are unlikely to incorporate these procedures into their standard of care until consistent substantial improvements over other treatment options are shown in controlled randomized clinical studies.

The strong observational data supporting the use of SVR and the validated randomized controlled studies which have yet to be performed provide an environment in which there is much room for improvement of these procedures. Enhancement of SVR outcomes will increase acceptance of this procedure and move it closer to the point where it will be available as a promising treatment option for large numbers of patients.

2.3 Regenerative Scaffolds Restore Tissue to Pre-Pathological State

One area in which improvement is needed and where it has the opportunity to shape the thinking behind SVR is the use of improved scaffolds. The clinical results discussed in the previous section demonstrate that the heart responds favorably when a scaffold is placed in it to alter its geometry. The scaffolds currently used in the procedures discussed above are made of passive materials such as Dacron or polyethylene which do not contribute work to the function of the heart. Instead of facilitating re-growth of heart tissue they become encapsulated by fibrous tissue and elicit a strong foreign body response (Xue & Greisler, 2003) (Robinson, Li, Mathison, Redkar, Cui, & Chronos, 2005).

In addition to restoring the geometry of the heart, the scaffolds used in recent research also restore lost cardiac tissue. It has been hypothesized that scaffolds should provide an environment in which cell infiltration and eventual remodeling can occur. This repopulation of the heart wall with healthy cardiac cells will in turn increase the amount of contractile muscle which contributes to the stroke work of the heart. Although chamber volume has been shown to be a more important clinical parameter than stroke work, enhancement of both of these parameters will likely give added benefit to patients (White, Norris, Brown, Brandt, Whitlock, & Wild, 1987).

It was recently demonstrated that scaffolds made from an extracellular matrix (ECM) result in improved regional mechanical function compared to Dacron scaffolds (Kochupura, et al., 2005) (Badylak,

Kochupura, Cohen, Doronin, Saltman, & Gilbert, 2006). The ECM scaffolds developed significant area contraction during systole eight weeks after implantation in canine right ventricles. The increased mechanical function corresponded with an increased number of myocytes in the ECM implant regions in contrast to fibroblast infiltration and collagen deposition in the Dacron implant regions. This active contraction in the ECM scaffold implant region occurred synchronously with the contraction of the adjacent myocardium demonstrating electrical integration with the surrounding tissue. Subsequent studies have also shown that the quantity of myocytes present in the implant region correlates with increased regional work (Kelly, Rosen, Schuldt, Kochupura, Doronin, & Potapova, 2009). These results suggest that remodeling of regenerative scaffolds by native cells leads to improvements in mechanical function.

2.4 Scaffold Mechanical Properties at Time of Implantation are Important

Whether scaffolds are intended to alter the geometry of the heart, restore damaged tissue, or both, the mechanical properties of the implanted scaffold are important. Since scaffolds are implanted into a load-bearing environment they must at the very least have the strength necessary to prevent an aneurysm from occurring. This means that their failure stress and failure strain must be greater than the stress and strain which they will experience in the heart.

In addition to having sufficient strength to resist failure, the stiffness of the scaffolds must also be appropriate. When a scaffold is implanted into the heart wall it will deform during diastole as the surrounding muscle relaxes and load is applied due to increasing pressure within the ventricle. The degree to which a scaffold deforms during this loading is described as its stiffness. The stiffness of the scaffolds must not be too high or cells which migrate onto them will be unable to sense the deformation which is occurring in adjacent heart tissue. Stiffness has been repeatedly shown to play an important role in the differentiation of progenitor cells and scaffolds with mismatched stiffness thus run the risk of harboring inappropriate cell types (Engler, Sen, Sweeney, & Discher, 2006) (Discher, Janmey, & Wang, 2005). Stiffness is also an important factor for any contractile myocytes which find their way to the scaffold through differentiation or by migration from the surrounding tissue. The stiffness of the scaffold must be such that the force exerted by the contraction of a critical number of myocytes is sufficient to deform the scaffold. Since any implant is subjected to substantial degradation when placed into the body the properties of the scaffold may be quite different by the time that a critical number of myocytes is present in the scaffold. Despite this, the mechanical properties of the scaffold at the time of implantation are an important starting point in the consideration of this issue.

2.5 Membrane Inflation Testing

The mode and complexity of the loading environments which occur throughout the body are greatly varied. Linear tissues such as tendons, bones, and many muscles can be considered to have load and deformation occurring predominantly in the direction that the load is applied. Planar tissues such as skin can be considered to have load and deformation occurring as a sum of principal forces in two orthogonal directions. Other tissues such as the lungs, many internal organs, and the heart, can be considered to be vessels pressurized by an internal fluid. While all of these assumptions are gross over-simplifications they are useful in developing a general understanding of each of the respective tissues.

As research into each tissue has progressed, mechanical testing methods for characterizing each type of loading environment have been developed. Uniaxial testing is the most popular method due to its ease of use and its applicability to many different tissue types. It is also a good first approximation even for tissue types which have very different loading environments *in vivo*. Biaxial testing is a more involved test method but it also gives insight into the mechanical properties of the material under a less simplified set of conditions.

A less frequently used mechanical testing method is membrane inflation. Membrane inflation testing is a method in which a planar sample is exposed to a pressurized fluid which inflates it to a "bubble" shape. The pressure of the fluid is monitored with a pressure transducer. The deformation of the sample is typically determined either by measuring the center displacement of the sample using a laser ((Billiar, Throm, & Frey, 2005), (Elsheikh & Anderson, 2005)) or a displacement transducer (Lim & Boughner, 1976), or by recording images of the profile of the sample and using image analysis software to determine the radius ((Slifka, Drexler, Wright, & Shandas, 2006), (Marra, Kennedy, Kinkaid, & Fillinger, 2006)). Membrane inflation testing has been used to characterize a wide variety of materials including ePTFE and latex (Slifka, Drexler, Wright, & Shandas, 2006), porcine aorta (Pearson, Philips, Hancock, Hashim, Field, & Richens, 2008) (Marra, Kennedy, Kinkaid, & Fillinger, 2006), human aortic valve (Lim & Boughner, 1976), corneal tissue (Elsheikh & Anderson, 2005), and living tissue equivalents (Billiar, Throm, & Frey, 2005).

Samples tested using the membrane inflation method are loaded as segments of a pressure vessel. When a scaffold is sutured to the heart wall it also becomes part of a pressure vessel and is subjected to loading as the chamber fills with blood. This project will compare the deformation of scaffolds when subjected to loading in the heart to that of scaffolds subjected to loading by the membrane inflation method.

2.6 Mechanical Properties of the Heart

The passive mechanical properties of the heart are often described using the relationship between pressure and volume during diastole. Pressure and volume are global parameters which can be easily measured non-invasively in a clinical setting and the parameters relating them are thus useful. The diastolic pressure-volume relationship has been characterized in a wide variety of ways ranging from simple linear descriptions to more complex exponential descriptions (Pasipoularides, Shu, Shah, Silvestry, & Glower, 2002) (Jaber, Lam, Meyer, & Redfield, 2007).

In many cases it is necessary to understand the local properties of a specific region on the heart wall rather than simply the global properties relating to the entire vessel. Local properties are expressed in terms of load and deformation. In order to estimate local properties a geometric model is required. The complex physiology of the heart is supported by an equally complex anatomy which has been modeled in many different ways. The gross geometry of the left ventricle has readily apparent similarities to simple geometric shapes and has been modeled as a cylinder, sphere, or ellipsoid. The geometry of the right ventricle does not have the same similarity to a simple geometry as that which is observed for the left ventricle. The most widely accepted model of the geometry of the right ventricle is Feneley's shell subtraction model (Feneley, Elbeery, Gaynor, & Gall Jr., 1990). In this model the entire

heart is considered to be a general ellipsoid containing the left ventricle as a smaller general ellipsoid. The right ventricle is modeled as the shell remaining when the ellipsoid representing the left ventricle is subtracted from the ellipsoid representing the heart.

In order to obtain more precise estimates of the passive mechanical properties of the heart, mathematical models have been developed. Using tools such as the Finite Element Method (FEM) geometric models can be constructed and local stresses can be estimated based on measurements of deformation (Wall, Walker, Healy, Ratcliffe, & Guccione, 2006). The detailed nature of these types of analyses makes them useful for studying the distribution of loading and deformation both spatially and temporally. These models are often used to model dynamic states of the heart and thus require a priori assumptions as to the passive mechanical properties of the heart.

High Density Mapping (HDM) is an imaging method which has been used to measure the strain on the surface of a beating heart *in vivo*. This method has previously been used to determine regional function in the isolated rabbit heart (Gaudette, Todardo, Krukenkamp, & Chiang, 2001) and the *in vivo* porcine heart (Azeloglu, Yun, Saltman, Krukenkamp, Chiang, & Chen, 2006). By combining the deformation analysis of HDM with estimation of tension using a geometric model, mechanical properties can be obtained.

The passive mechanical properties of the heart have also been characterized through mechanical testing of excised samples of heart tissue (Nagueh, Shah, Wu, Torre-Amione, King, & Lahmers, 2004). Given proper preservation of the tissue the parameters associated with standard mechanical testing methods can be obtained. This approach is beneficial since the passive behavior of the native tissue is directly tested, however changes which occur in the tissue from its *in vivo* to *in vitro* state may have substantial effects on its properties.

2.7 Tissue Engineering Can be used to Develop Scaffolds with Improved Mechanical Properties

Scaffolds for SVR are either fabricated from raw materials or developed from allogeneic tissues. Fabricated scaffolds are advantageous in that their structure can often be carefully controlled during manufacturing to produce scaffolds with a wide range of properties. However, they are often produced from synthetic materials which interact with the implant site in at best a neutral manner.

The source for scaffolds developed from allogeneic tissues is often a membrane which makes up the wall of a cadaveric organ. Since these scaffolds are derived from a physiological source they are thought to interact more favorably with the tissue and cells in the implant site. However, these biological membrane scaffolds are harvested from a donor and must be treated extensively to avoid severe reactions by the immune system. Traditionally this treatment has involved harsh cross-linking chemicals which also mask the biologically active regions of the material. Recent advances have enabled processing of biological membrane scaffolds in such a way that their biological activity is retained, thus giving them a significant advantage over fabricated scaffolds. Despite these advances, a remaining disadvantage is that the mechanical properties are determined by that of the source tissue and the "tailorability" of fabricated scaffolds has not been possible.

Recently, cell mediated remodeling has been investigated as a means to alter the mechanical properties of biological membrane scaffolds. Many experimental models have been developed to study how the mechanical properties of scaffolds change as they are remodeled by cells. A number of studies have been able to show that changes in scaffold stiffness are associated with increasing the length of time that cells are cultured on the material. Scaffolds constructed of collagen fibers embedded in a collagen gel showed significantly higher stiffness when seeded with fibroblasts for 25 days compared to unseeded scaffolds (Gentleman, Lay, Dickerson, & Nauman, 2003). Smooth muscle cells cultured on collagen scaffold for 10 weeks were found to induce an approximately 15-fold increase in stiffness compared to unseeded controls (Kim, Nikolovski, Bonadio, & Mooney, 1999).

Different cell types have been found to have widely varied effects on scaffold stiffness due to the different mechanisms by which the cells remodel the material. Small intestinal submucosa (SIS) seeded with muscle derived stem cells was found to become significantly more compliant than unseeded scaffolds after 10 days of culture (Long, Nagatomia, Chancellor, & Sacks, 2006) (Lu, et al., 2005). The authors proposed that this was a result of degradation of the scaffold by MMP-1 which was found to be strongly expressed by the cells. On the other hand, when this same material was seeded with fibroblasts, collagen expression was found to increase in response to increasing levels of stretch and frequency applied to the scaffold during culture (Gilbert, Stewart-Akers, Sydeski, Nguyen, Badylak, & Woo, 2007). Although the variation between samples made it difficult to perform statistical comparisons there was a definite trend between increasing collagen expression and scaffold stiffness. Table 1 provides a summary of key parameters for several studies in which the stiffness of biological scaffolds was altered by exposure to cell culture conditions.

Table 1: Review of studies in which the stiffness of biological scaffolds was altered by exposure to cell culture conditions

Substrate	Cell Type	Incubation Time	Effect on Stiffness	Reference
Collagen Fiber in Collagen Gel	Fibroblasts	25 Days	↑	(Gentleman, Lay, Dickerson, & Nauman, 2003)
Collagen Scaffold	Smooth Muscle Cells	10 Weeks	↑	(Kim, Nikolovski, Bonadio, & Mooney, 1999)
Small Intestinal Submucosa	Muscle Derived Stem Cells	10 Days	↓	(Long, Nagatomia, Chancellor, & Sacks, 2006)
Small Intestinal Submucosa	Muscle Derived Cells	10-25 Days	↓	(Lu, et al., 2005)
Small Intestinal Submucosa	Fibroblasts	3 Days	N/A	(Gilbert, Stewart-Akers, Sydeski, Nguyen, Badylak, & Woo, 2007)
Small Intestinal Submucosa	Primary Tendon Cells	16 Days	↑	(Androjna, Spragg, & Derwin, 2007)

The striking differences found by these groups when working with various cell culture conditions can be highlighted by looking at two examples. Androjna and colleagues (Androjna, Spragg, & Derwin, 2007) applied uniaxial cyclic strains to small intestinal submucosa scaffolds cultured with or without primary tendon cells for several weeks. Through continuous monitoring of the stress and strain applied to the scaffolds the stiffness could be determined for each day in culture, and it was found that the daily increase in stiffness was substantially higher for scaffolds cultured in the presence of cells. This was attributed to the presence of aligned cytoskeletons as well as to deposition of new extracellular matrix. In another study using the same scaffold material but a different cell type and media formulation the opposite result was found (Long, Nagatomia, Chancellor, & Sacks, 2006). Equibiaxial loads of 1 MPa were applied to the samples and the area strain was determined. It was found that the areal strains were significantly higher for scaffolds cultured with cells. The researchers investigated the cause for this change by incubating scaffolds in the enzyme collagenase for increasing amounts of time and found that this had a similar effect to culturing with cells. Because collagenase was found to be secreted by the cells, the authors attributed the decrease in scaffold stiffness to degradation of the scaffold by this cell produced collagenase.

One way in which the remodeling of scaffolds by cells can be magnified is to stimulate production of extracellular matrix proteins using growth factors. Fibroblasts are a readily available cell type which has been reported to have increased collagen deposition when cultured with ascorbic acid (Tullberg-Reinert & Jundt, 1999), (Chan, Lamande, Cole, & Bateman, 1990), (Ishikawa, Kondo, Okada, Miyachi, & Furmira, 1997), (Yamamoto, Muto, Murakami, & Akiyama, 1992). This increased collagen deposition occurs as the cells are able to more efficiently incorporate pro-collagen secreted into the culture media into collagen fibrils in the cell layer (Chan, Lamande, Cole, & Bateman, 1990). A wide range of ascorbic acid concentrations have been reported from 0.25 mM (Chan, Lamande, Cole, & Bateman, 1990) to 1 mM (Ishikawa, Kondo, Okada, Miyachi, & Furmira, 1997).

Chapter 3: Hypothesis

As described in the previous chapter the stiffness of cardiac scaffolds is an important parameter which may contribute to regeneration of new cardiac tissue. The goal of this project is to demonstrate that stiffness can be both characterized and altered *in vitro*. This goal will be accomplished through examination of two hypotheses.

As noted in the previous chapter the loading of a cardiac scaffold implanted into the heart wall can be modeled as that of pressure vessel. It was also noted that the membrane inflation *in vitro* mechanical testing method loads samples in a similar way. It was therefore hypothesized that **the stiffness of scaffolds measured using membrane inflation testing will be similar to the stiffness of scaffolds measured immediately upon implantation into the heart**. This hypothesis was investigated by analyzing data previously obtained from an *in vivo* study in which two materials, Dacron and an extracellular matrix (porcine urinary bladder matrix), were implanted into canine right ventricles. Before closing the surgical site the deformation of the scaffold was measured using high density mapping (HDM) and the pressure within the vessel was measured using a transducer within a catheter. The tension applied to the scaffolds was estimated by applying a modified shell subtraction model to the right ventricular wall. The stiffness of each scaffold material was determined and compared to that obtained using the membrane inflation method.

The second hypothesis was that **biological membrane scaffolds subjected to long term incubation in culture media as well as culture with fibroblasts with or without ascorbic acid will undergo remodeling, thus altering material stiffness**. In order to investigate this hypothesis a biological scaffold was subjected to several cell culture conditions and the resulting changes in biochemical composition and mechanical properties were examined. Collagen is the primary structural protein in the scaffolds and the amount of acid soluble and acid insoluble collagen contained in each sample was thus determined. The mechanical testing methodology developed in the first hypothesis was used to compare the mechanical properties of the scaffolds. The change in mechanical properties from the control scaffolds and the correlation between these mechanical properties and collagen were examined.

Chapter 4: Materials and Methods

The procedures used to evaluate each of the hypotheses examined in this study are described in this chapter.

4.1 Measurement of Scaffold Deformation and Loading during *In Vivo* Testing and Membrane Inflation Testing

Comparison of stiffness measured *in vivo* to that measured using membrane inflation testing was performed by determining the deformation and loading of scaffolds in both conditions. Deformation was characterized by the area stretch ratio in both cases and load was characterized by applying the law of Laplace. The methods used to characterize *in vivo* stiffness will be described first, followed next by a description of the methods used to determine stiffness via membrane inflation testing, and lastly by a description of the analysis methods used to compare these two approaches.

4.1.1 *In Vivo* Testing: Experimental Procedure

Studies performed at Stony Brook University (Kelly, Rosen, Schuldt, Kochupura, Doronin, & Potapova, 2009) generated the *in vivo* scaffold deformation data used in this analysis. Eight adult mongrel dogs were sedated and a left thoracotomy was performed according to a protocol approved by the Stony Brook University Institutional Animal Care and Use Committee. A full thickness defect was created in the right ventricle by clamping an approximately $2cm^2$ region of the free wall and excising the clamped tissue. The right ventricle was chosen as a first model for evaluation of the patches because it provides a more moderate loading environment than the left ventricle. An extracellular matrix (ECM) graft made from urinary bladder matrix (UBM) was used to repair the defect in four dogs and a Dacron graft was used to repair the defect in the other four dogs.

Global cardiac geometry was measured prior to implantation of the scaffolds using sonomicrometry (Kochupura, et al., 2005). Briefly, ultrasonic transducer crystals were placed along three axes of the right ventricle as shown in Figure 1:. The three axes run 1) from the free wall to the septum, 2) from the anterior wall to the posterior wall, and 3) from the base to the apex. The mean and standard deviation of each axis were determined based on measurements from two full heart beats of eight separate hearts.

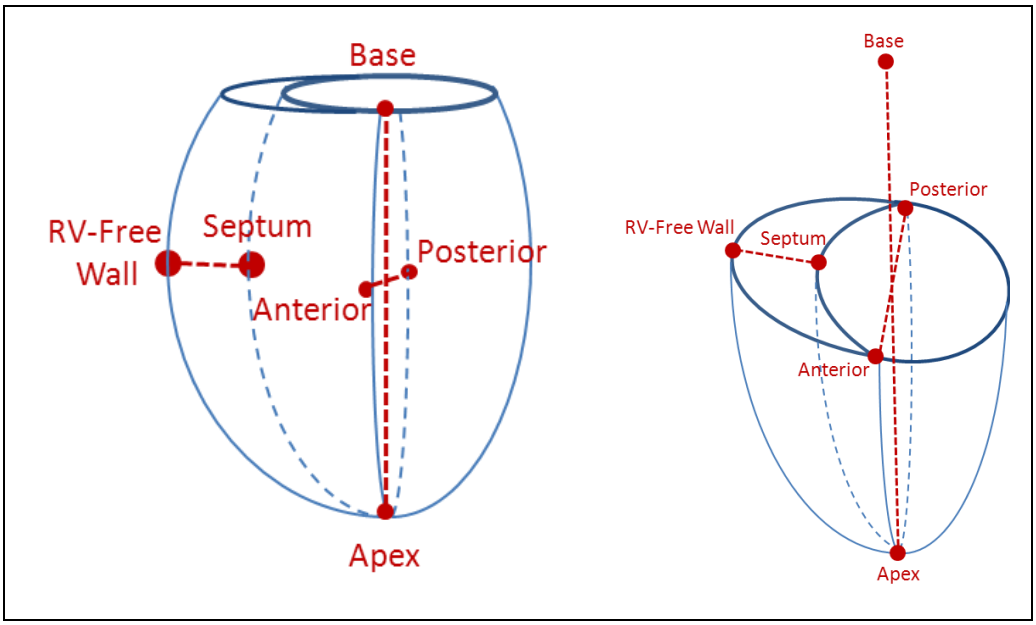

Figure 1: Three different axes within the right ventricle as defined by placement of ultrasonic transducer crystals. The axes run 1) from the free wall to the septum, 2) from the anterior wall to the posterior wall, and 3) from the base to the apex.

Mechanical function of the implant region was evaluated after 15 minutes of recovery. A pressure transducer (Millar, Houston, TX) was placed in the right ventricle and data was acquired at a rate of 125Hz. In addition, silicon carbide particles were sprinkled on the surface of the implanted scaffold to create a random light intensity pattern. A high speed camera was focused on the speckles and images were acquired at a rate of 250 frames per second.

The images were analyzed using High Density Mapping (HDM), a method which measures regional displacement over time. As shown in Figure 2, a region of interest (ROI) was selected from the acquired image and divided into sub-images of equal size, each with its own unique light intensity pattern. A series of Fourier transforms was applied to each sub-image and used to determine the displacements (*u* and *v*) from one frame to the next based on the *x* and *y* coordinates describing the peak of the light intensity pattern (Kelly, Rosen, Schuldt, Kochupura, Doronin, & Potapova, 2009).

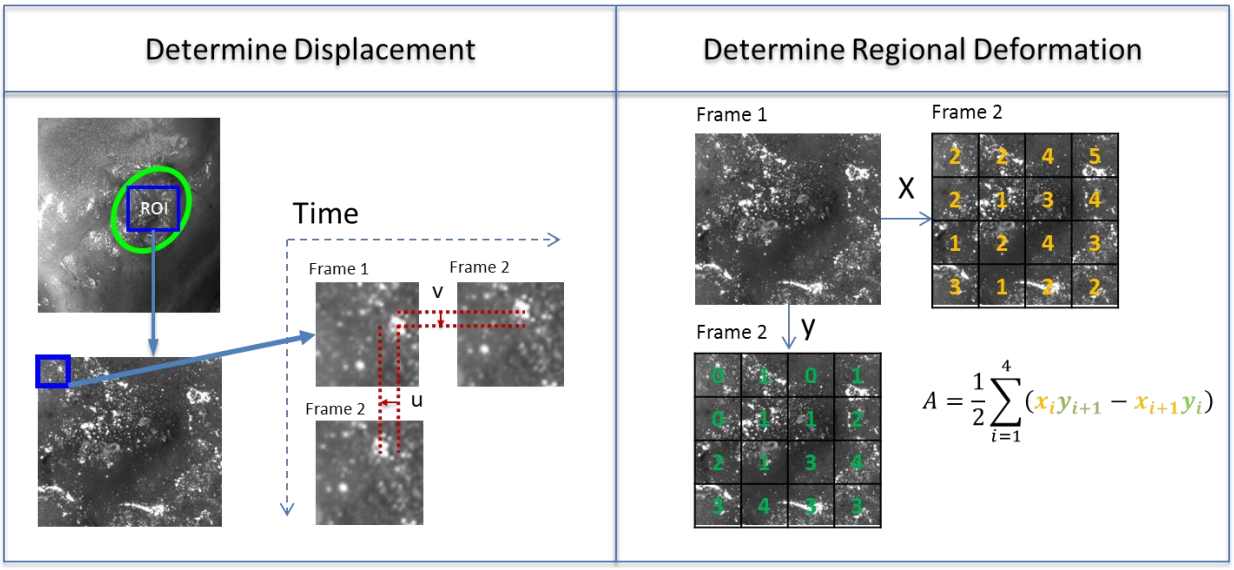

Figure 2: High Density Mapping was used to determine deformations of cardiac scaffolds in the *in vivo* canine heart. A region of interest (ROI) with a unique light intensity pattern that could identify it in all subsequent images was selected. The region of interest was divided into sub-images and a Fourier transform was used to determine the x and y coordinates of the light intensity peak in each sub-image. The coordinates for each sub-image were compared to the coordinates for the same sub-image in the following frame and the resulting displacements were determined. The area of each set of four adjacent sub-images was computed and all areas were summed together to determine the total change in area from the previous frame.

4.1.2 *In* Vivo Testing: Scaffold Deformation

The change in area for the Region of Interest (ROI) between two consecutive frames was determined using the displacements of four neighboring sub-images as shown in the equation below:

$$A = \frac{1}{2}\sum_{i=1}^{4}(x_i y_{i+1} - x_{i+1} y_i) \quad (1)$$

where *i* refers to the individual sub-images and *x* and *y* refer to the coordinates of the sub-images. The total change in the ROI area for each frame was calculated by summing the area change of that frame with the area change for all previous frames. The area stretch ratio was determined by dividing the deformed area (A) calculated for a given frame by the undeformed area (A_0) calculated for the initial frame.

$$\lambda_{Area} = \frac{A}{A_0} \quad (2)$$

This analysis of regional deformation was carried out for each set of frames acquired throughout the loading cycle with each frame being associated with a corresponding value for pressure. The loading curve was defined from end diastole to the point at which area stretch ratio ceases to increase.

4.1.3 *In Vivo* Testing: Scaffold Loading

The loading within a vessel wall may be described by relating the geometry of the vessel to the pressure within the vessel according to the Law of Laplace. Conceptually, the Law of Laplace states that

for static equilibrium to exist, the force acting on the vessel wall must be equal to the force acting within the vessel wall.

To illustrate this, a wall segment on the surface of a vessel was considered. This segment had sides of length dS_1 and dS_2 which are defined by two perpendicular sets of radii of curvature (R_1, R_2) and angles of rotation ($d\theta_1$, $d\theta_2$). Pressure within the vessel (P) resulted in two perpendicular stresses (σ_1, σ_2) acting on the wall in the direction of each radius of curvature as shown in Figure 3 below.

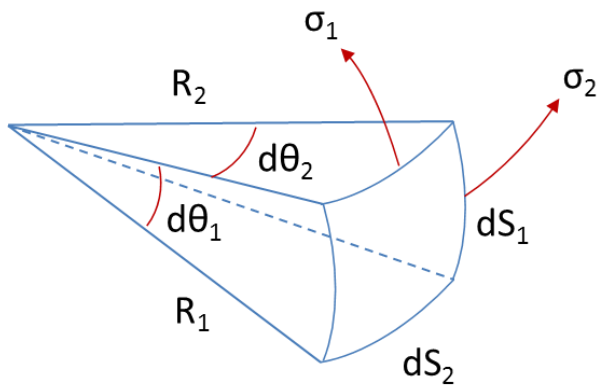

Figure 3: Schematic of a segment of a pressure vessel wall. The wall has perpendicular sides of lengths dS_1 and dS_2. The sides of the wall segment are defined by corresponding angles ($d\theta_1$, $d\theta_2$) and radii of curvature (R_1, R_2). A stress component (σ_1, σ_2) acts perpendicular to each side of the wall segment.

The component of stress within a cross-section of the wall which balanced the force applied by pressure was represented by the following expression:

$$\sigma \sin\frac{d\theta}{2} \tag{3}$$

The determination of this term is illustrated in Figure 4 below:

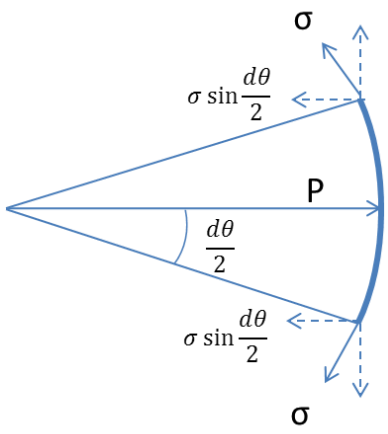

Figure 4: Cross section of a segment of a pressure vessel wall defined by an angle ($d\theta/2$). The stress (σ) component [$\sigma sin(d\theta/2)$] within the wall counteracts the pressure (P) acting on the wall.

A force balance applied to the wall segment resulted in the following expression in which the thickness of the wall segment is represented by the variable *t*:

$$PdS_1dS_2 = tdS_2 2\sigma_1 \sin\frac{d\theta_1}{2} + tdS_1 2\sigma_2 \sin\frac{d\theta_2}{2} \quad (4)$$

This expression was further simplified by recognizing that sin(θ) = θ for small values of θ, that S=Rθ, and by canceling out the constants.

$$PR_1\theta_1 R_2\theta_2 = tR_2\theta_2\sigma_1\theta_1 + tR_1\theta_1\sigma_2\theta_2 \quad (5)$$

Each side of the equation was divided by common terms as shown in the equation below:

$$\frac{PR_1\theta_1 R_2\theta_2}{tR_1\theta_1 R_2\theta_2} = \frac{tR_2\theta_2\sigma_1\theta_1}{tR_1\theta_1 R_2\theta_2} + \frac{tR_1\theta_1\sigma_2\theta_2}{tR_1\theta_1 R_2\theta_2} \quad (6)$$

This resulted in the expression below:

$$\frac{P}{t} = \frac{\sigma_1}{R_1} + \frac{\sigma_2}{R_2} \quad (7)$$

The tension (*T*), or force per unit length, was determined rather than stress by utilizing the following relationship between the two terms:

$$\sigma = \frac{T}{t} \quad (8)$$

This resulted in the following expression:

$$P = \frac{T_1}{R_1} + \frac{T_2}{R_2} \quad (9)$$

For the right ventricle, pressure and radius of curvature were either measured directly or calculated from directly measured data, and thus two unknown terms (T_1 and T_2) still remained. As will be discussed shortly, the right ventricle was modeled as a prolate ellipsoid with a circumferential radius of curvature and a radial radius of curvature. At the outermost point of this ellipse, the circumferential radius of curvature approaches zero and the radial radius of curvature defines both radii of curvature of a wall segment at this point. To determine the tension at this point, a segment similar to the one illustrated in Figure 3 was considered. This segment had sides of equal length ($dS_1 = dS_2$) and equal radii of curvature ($R_1 = R_2$). It follows from these two equivalencies that the two angles are also equal ($\theta_1 = \theta_2$). If a cross-section such as the one illustrated in Figure 4 is considered in the direction of each radius of curvature, the following two force balances are obtained.

$$P = \sigma_1 \sin\frac{d\theta}{2} \qquad\qquad P = \sigma_2 \sin\frac{d\theta}{2} \tag{10}$$

By setting both of these expressions equal to each other it was found that the stress was the same in both directions.

$$\sigma_1 \sin\frac{d\theta}{2} = \sigma_2 \sin\frac{d\theta}{2} \tag{11}$$

$$\therefore\ \sigma_1 = \sigma_2 \tag{12}$$

A single value for stress was thus substituted into equation (7) to obtain the following expressions.

$$\frac{P}{t} = \frac{\sigma}{R} + \frac{\sigma}{R} = \frac{1}{R}(2\sigma) \tag{13}$$

$$\therefore\ \sigma = \frac{PR}{2t} \tag{14}$$

By substituting tension for stress, the following expression is obtained.

$$\frac{T}{t} = \frac{PR}{2t} \therefore T = \frac{PR}{2} \tag{15}$$

This equation enabled the tension at the outermost point of the right ventricular free wall to be calculated based on the pressure within the ventricle and the radius of curvature at this point. The pressure within the ventricle was determined based on measurements which were acquired directly throughout each heartbeat as described previously. The radius of curvature was estimated based on a modified form of the shell subtraction model. In the shell subtraction model the entire heart is modeled as a general ellipsoid with the left ventricle as a smaller general ellipsoid within it. The right ventricular free wall is thus the surface of revolution created by rotating the arc running through the base, apex, and right ventricular free wall sonomicrometry transducers by ± 90°.

The general case of modeling the left ventricle as a general ellipsoid was refined by first noting that only one dimension was measured for the mid-plane of the left ventricle. The left ventricle was thus considered to be a prolate ellipsoid with a minor axis given by the anterior-posterior dimension and the major axis given by the base-apex dimension. The geometry of the left ventricle was further simplified to that of a sphere based on the observation that no statistically significant difference existed between the average length of the anterior-posterior dimension and the average length of the base-apex dimension. The diameter of this sphere was thus defined as the average of the lengths of the anterior-posterior dimension and the base-apex dimension.

The right ventricle was then modeled as a spherical cap with a base diameter which was equal to the diameter of the left ventricle. The height of the spherical cap was given by the sum of the length

of the right ventricular free wall-septum dimension and half of the diameter of the left ventricle. The geometric modeling of the right ventricle is illustrated in Figure 5 below:

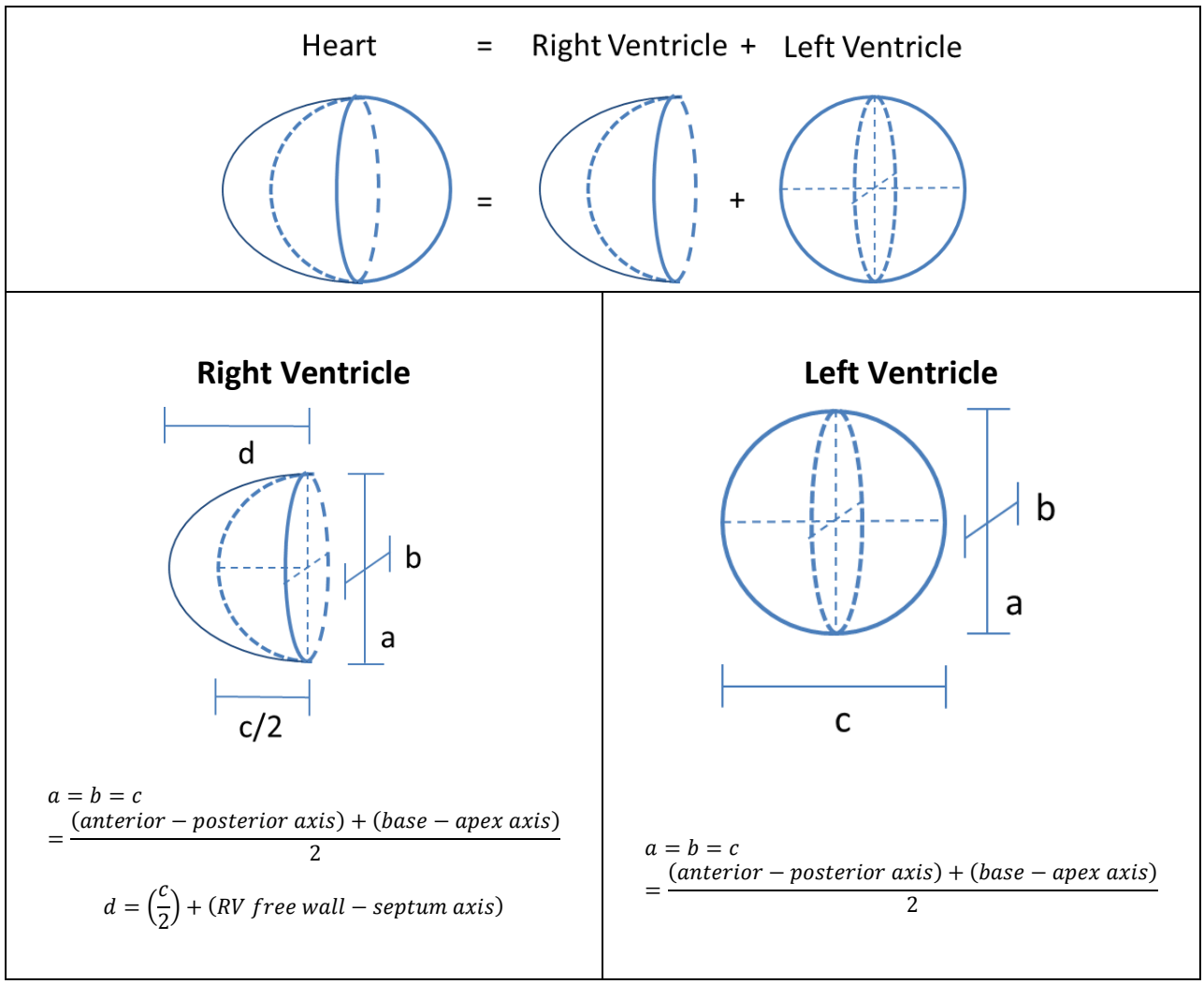

Figure 5: The geometry of the left ventricle is modeled as a sphere. The geometry of the right ventricle is modeled as a spherical cap.

The radius of curvature of the ellipsoid used to model the right ventricle was determined by considering the ellipse formed by taking a cross-section of the ellipsoid along its major radius of curvature. Standard geometric characteristics of an ellipse were then utilized as shown in Figure 6.

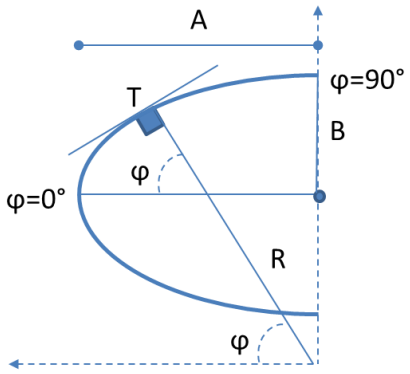

Variable	Description
A	Semi-major axis
B	Semi-minor axis
e	Eccentricity
T	Tangent line to surface of curve
R	Radius of curvature
ϕ	Geodetic latitude

Figure 6: Characteristic parameters of a general ellipse used to determine radius of curvature of the right ventricle.

A fundamental characteristic of any ellipse is its eccentricity, which describes the degree to which it varies from a spherical shape. The eccentricity was calculated from the semi-major axis (*a*) and the semi-minor axis (*b*) as follows:

$$e = \frac{\sqrt{A^2 - B^2}}{A} \tag{16}$$

The eccentricity of the ellipse was used to calculate the radius of curvature (*R*) which was defined as the line originating on the y-axis and which is perpendicular to the tangent line at any point on the surface of the curve. The magnitude of the radius of curvature varies as a function of the geodetic latitude (φ) which is the angle formed between the radius of curvature and the x-axis and which defines the point along the curve surface for which the radius of curvature is calculated. The radius of curvature was calculated as follows:

$$R = \frac{A}{\sqrt{1 - e^2 \sin\varphi^2}} \tag{17}$$

The radius of curvature is unique for each point along the surface of the curve and has its maximum value at the 'pole' of the ellipsoid (φ=90°) and its minimum value at the 'equator' of the ellipsoid (φ=0°). Analysis of tension in the right ventricle was performed for the outermost point on the right ventricular free wall, and the radius of curvature at a geodetic latitude of 0° was thus considered. The radius of curvature at this point was found to simplify to be equivalent to the length of the semi-major axis as shown in the equation below.

$$R = \frac{A}{\sqrt{1 - e^2 sin^2 0°}} = A \tag{18}$$

The tension within the right ventricle can thus be computed using the following equation:

$$T = \frac{Pd}{2} \tag{19}$$

Using the methods described in this section, tension was calculated at each point for which data were acquired from end diastole to the point at which maximum pressure was reached. In order to apply the equations developed in this section, several assumptions were made.

- The pressure within the right ventricle was uniform and the only load on the ventricular free wall.
- The equation for tension developed in this section was only valid for thin-walled vessels in which the tension is considered to be the same throughout the thickness of the sample. For thick-walled vessels, bending effects would result in an uneven distribution of tension across the thickness of the wall. The right ventricle was considered to be a thin-walled vessel in this analysis since the thickness of the ventricular wall was small in comparison to the radius of curvature.
- The tension in a scaffold implanted in the right ventricular free wall was the same as the tension in the right ventricular free wall.
- The right ventricular free wall was transversely isotropic, homogenous, and linearly elastic. The scaffold materials were also considered to be transversely isotropic, homogenous, and linearly elastic. Transverse isotropy implies that the properties of the materials are consistent within the plane of loading. Homogeneity implies that the properties of the material are the same at all points. Linear elasticity implies that a linear relationship exists between stress and strain.

4.1.4 Membrane Inflation Testing: Experimental Procedure

Dacron and ECM were tested using a novel membrane inflation device previously described elsewhere (Billiar, Throm, & Frey, 2005) and used in several other studies (Ahlfors & Billiar, 2007) (Throm, Liu, Lock, & Billiar, 2010) (Balestrini & Billiar, 2006). Briefly, samples were secured to the surface of a cylindrical chamber with a 5mm radius. This chamber was then infused with room temperature water via a syringe pump at a rate of 1 mL/minute. The pressure inside the chamber was measured using a pressure transducer and the displacement at the center of the sample was measured using a laser displacement system. Pressure and displacement measurements were acquired simultaneously at a rate of 10 Hz using a LABVIEW (National Instruments, Austin, TX) program. Data was recorded for the first ten loading cycles of each sample and data from the tenth cycle was used for further analysis.

The thickness of each sample was measured prior to testing using the laser displacement system. A metal disk weighing 1.3 g was placed at the center of the sample to displace water present in the sample and give more consistent measurements. Data were recorded for two minutes and the sample thickness reported was the final equilibrium value that was reached.

4.1.5 Membrane Inflation Testing: Scaffold Deformation

The radius of curvature of a spherical cap was determined by considering a spherical cap with a base of a given radius (*a*) and height (*w*). This spherical cap was a segment of a larger sphere with radius *R* as shown in Figure 7 below.

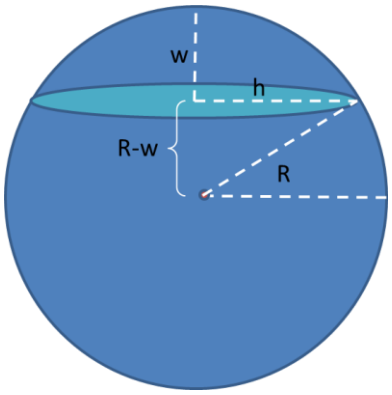

Figure 7: The radius of curvature (*R*) of a spherical cap can be determined based on the height of the spherical cap (*w*) and the radius of its base (*a*).

The radius of curvature was calculated based on the Pythagorean Theorem which states that the square of the length of a triangle's hypotenuse is equal to the sum of the squares of each of the sides. For the spherical cap shown above, this expression was:

$$R^2 = (R - w)^2 + h^2 \tag{20}$$

Expanding this expression and rearranging the terms yielded:

$$R^2 = R^2 - 2wR + w^2 + h^2 \tag{21}$$

$$\therefore 2wR = w^2 + h^2 \tag{22}$$

Solving for R yielded the following expression:

$$R = \frac{w^2 + h^2}{2w} \tag{23}$$

The radius of curvature was used to calculate the surface area (*A*) of a spherical cap as given by the following geometric relationship:

$$A = 2w\pi R = \frac{2w\pi(w^2 + h^2)}{2w} = \pi(w^2 + h^2) \tag{24}$$

The area stretch ratio was defined as the deformed area divided by the undeformed area as shown below:

$$\lambda_{Area} = \frac{A}{A_0} = \frac{\pi(w^2 + h^2)}{\pi h^2} = \frac{w^2 + h^2}{h^2} \tag{25}$$

Linear strain was also determined for each data point based on the geometric relationship that exists between the arc length of a cross-section of a sample (*S*), the angle which the arc spans (θ), and the radius of curvature (*R*) as illustrated in Figure 8 below:

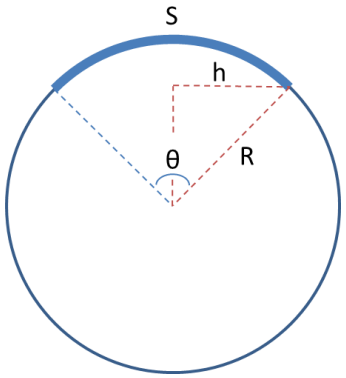

Figure 8: The arc length (S) of a cross section of a sample is related to the angle which the arc spans (θ), the radius of curvature (R), and the radius of the base of the sample (h).

The length of an arc is related to the angle (in radians) which the span of the arc creates with the center of the circle as shown in the equations below:

$$\frac{S}{Circumferance} = \frac{\theta}{2R} \tag{26}$$

$$\frac{S}{2\pi R} = \frac{\theta}{2R} \tag{27}$$

Simplification yielded the following relationship between the arc length, radius of curvature, and the angle with the center of the circle.

$$S = R\theta \tag{28}$$

The central angle was determined from measured parameters using the trigonometric relationship shown below:

$$\theta = 2\sin^{-1}\frac{h}{R} \tag{29}$$

The arc length was thus:

$$S = R\theta = R2\sin^{-1}\frac{h}{R} \tag{30}$$

The average stretch ratio along a given meridian was determined by dividing the instantaneous arc length by the initial arc length (S_0) as given in the following equation:

$$\lambda = \frac{s}{s_0} = \frac{R2\sin^{-1}\frac{h}{R}}{2h} = \frac{R\sin^{-1}\frac{h}{R}}{h} \tag{31}$$

Infinitesimal strain was calculated from the stretch ratio using the following equation:

$$\varepsilon = \lambda - 1 \tag{32}$$

Displacement within the sample varies from its maximum value at the center of the spherical cap to its minimum value at the boundaries of the spherical cap which are fixed and where no displacement occurs. For a transversely isotropic, homogenous material, the change in arc length thus occurs due to strain at the center of the arc. This expression for strain is thus only valid at the center of the spherical cap where displacement was measured.

4.1.6 Membrane Inflation Testing: Scaffold Loading

As demonstrated in equation (9) of section 4.1.3, the tensions in a vessel wall are related to the pressure within the vessel (P) and the radii of curvature (R_1, R_2):

$$P = \frac{T_1}{R_1} + \frac{T_2}{R_2} \tag{33}$$

A spherical cap is a segment of a sphere and thus a single radius of curvature was calculated ($R_1 = R_2$) as demonstrated in the previous section. The pressure applied to samples during membrane inflation testing was directly measured. The values for each of the tensions are thus unknowns and were found by considering a sphere for which a cut was made at the equator. For this configuration only one tension acted to balance the pressure exerted on the cross-sectional area of the sphere as shown in Figure 9 below.

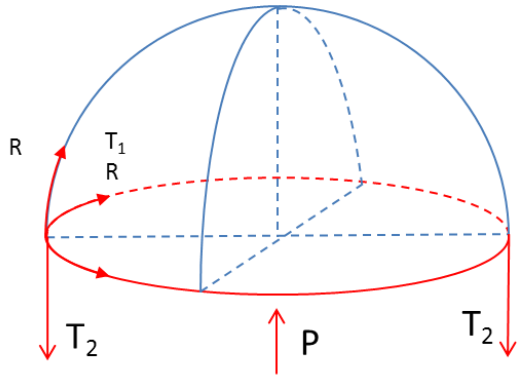

Figure 9: A cross section of a sphere is taken at the equator where only one of the tension components (T_2) counteracts the pressure (P) acting over the cross-sectional area of the vessel. Since the geometry of this shape has been defined as a sphere, the radius of curvature (R) is the same in both directions.

Applying the principle that the force acting on the wall must be equal to the force acting within the wall, the following force balance was obtained:

$$P\pi R^2 = T_2 2\pi R \tag{34}$$

Rearranging terms yielded the following expression for T_2:

$$T_2 = \frac{PR}{2} \tag{35}$$

This value for T_2 was substituted into the general form of the Law of Laplace to obtain the following expression:

$$P = \frac{T_1}{R} + \frac{PR}{2R} \tag{36}$$

Simplification resulted in the following expression for T_1:

$$T_1 = \left(1 - \frac{1}{2}\right) PR = \frac{PR}{2} \tag{37}$$

Thus, for this case in which the two radii of curvature were equal, the two tensions were also equal and could be defined by a single expression:

$$T_1 = T_2 = \frac{PR}{2} \tag{38}$$

This analysis was performed for each data point acquired during the tenth loading cycle of each sample measured using membrane inflation testing. Due to the nonlinear relationship between the radius of curvature and the center displacement, the tension values obtained at low displacements also varied non-linearly with center displacement. The radius of curvature was found to vary linearly with displacement for displacement values greater than 0.2 mm. The linear region was thus defined as containing all points with a displacement greater than or equal to 0.2 mm. Only data within the linear region was used for analysis. Again, it was assumed that the samples analyzed using membrane inflation testing were transversely isotropic and homogenous.

4.1.7 Comparison of Mechanical Properties of Scaffolds Determined During *In Vivo* Testing and Membrane Inflation Testing

The loading and deformation of samples tested *in vivo* or by membrane inflation testing were expressed with the parameters of tension and area stretch ratio respectively. Comparisons between the results obtained by the two testing methods were thus made by calculating the "stiffness" for each sample, which was defined as the tension divided by the area stretch ratio as shown in the equation below:

$$Stiffness = \frac{Tension}{Area\ Stretch\ Ratio} \tag{39}$$

A numerical value for this expression was obtained from the measured data using the slope determination method described in ASTM D695-08. Briefly the slope and intercept of the linear portion of the curve were calculated and the offset strain (λ_{offset}) was determined using the following relationship:

$$\lambda_{offset} = \frac{-intercept}{slope} \tag{40}$$

The stiffness at a given point ($Stiffness_i$) was calculated by dividing tension at that point (T_i) by the area stretch ratio at that point (λ_i) subtracted from the offset strain as shown in the equation below:

$$Stiffness_i = \frac{T_i}{\lambda_i - \lambda_{offset}} \tag{41}$$

To obtain an accurate value for this parameter, the number of points in the data set was determined and stiffness was calculated at 10% intervals between the beginning and end of the data set. These values were averaged to yield the stiffness of the sample.

$$Stiffness_{Average} = \frac{1}{9}\sum_{i=1}^{i=9} \frac{T_i}{\lambda_i - \lambda_{offset}} \tag{42}$$

The calculation of stiffness is illustrated in Figure 10:

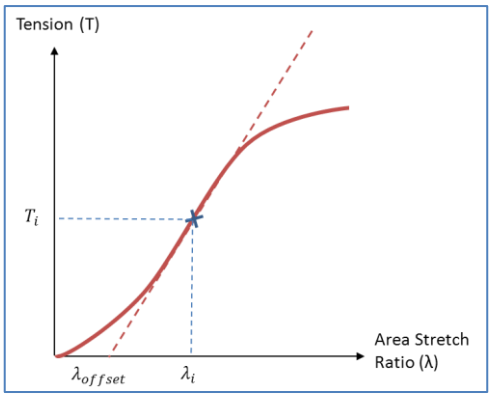

Figure 10: Stiffness was calculated by dividing the tension along the linear portion of the tension-area stretch ratio curve by the corresponding area stretch ratio.

4.1.8 Membrane Inflation Testing: Comparison to Other Studies

The elastic modulus of the samples characterized by membrane inflation testing was computed in order to compare the results of this study to other characterizations of the mechanical properties of ECM and Dacron found in the literature. An expression for the modulus was obtained by considering a rectangular element with sides of lengths *a*, *b*, and *c* in the *x*, *y*, and *z* directions respectively. Figure 11

shows a schematic of this element to which two stresses (σ_x, σ_y) are applied in the *x* and *y* directions respectively.

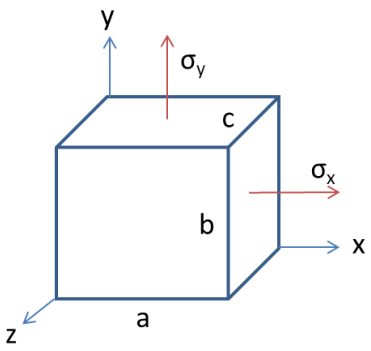

Figure 11: A schematic of a rectangular element to which stress (σ_x, σ_y) are applied in the x and y directions respectively

The stresses are defined as the force (F) applied over the surface area of a side of the element.

$$\sigma_x = \frac{F_x}{A_x} = \frac{F_x}{bc} \qquad \sigma_y = \frac{F_y}{A_y} = \frac{F_y}{ac} \tag{43}$$

The stress in the x-direction results in elongation of the element in the x-direction and contraction of the element in the y direction. This is shown schematically for the surface of the element in the x-y plane in Figure 12.

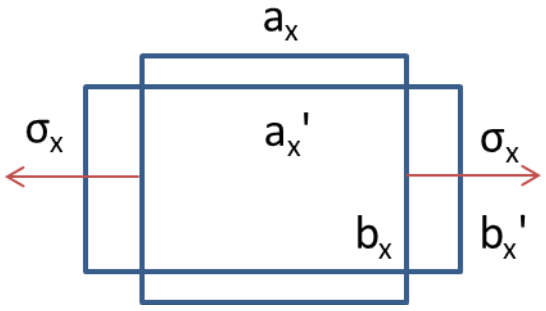

Figure 12: A schematic of the surface of the element shown in Figure 11 in the *x*-*y* plane. The deformation caused by a stress in the *x*-direction is shown. Elongation of the surface in the x-direction results in lengthening of one side from a length of a_x to a length of a_x'. Contraction of the surface in the y-direction results in shortening of one side from a length of b_x to a length of b_x'.

The elongation of the surface in the x-direction and the contraction of the surface in the y-direction can be described by calculating the respective primary strain in the x-direction (ε_{x1}) and secondary strain in the y-direction (ε_{y2}):

$$\varepsilon_{x1} = \frac{a'_x - a_x}{a_x} \qquad \varepsilon_{y2} = \frac{b'_x - b_x}{b_x} \tag{44}$$

These strains are related to the stress in the x-direction through the elastic modulus (*E*) and Poisson's ratio (*v*) by the following relationships:

$$\varepsilon_{x1} = \frac{\sigma_x}{E} \qquad \varepsilon_{y2} = -\nu\varepsilon_{x1} = -\nu\frac{\sigma_x}{E} \tag{45}$$

In a similar manner, the stress in the y-direction results in elongation of the element in the y-direction and contraction of the element in the x-direction. This is shown schematically for the surface of the element in the x-y plane in Figure 13.

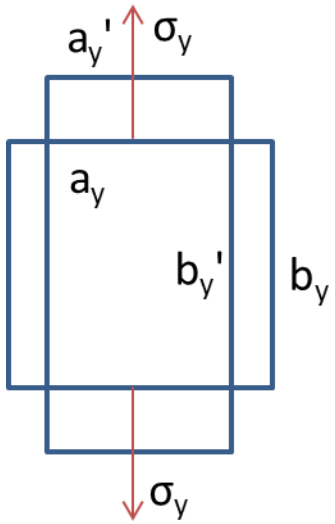

Figure 13: A schematic of the surface of the element shown in Figure 11 in the *x-y* plane. The deformation caused by a stress in the *y*-direction is shown. Elongation of the surface in the y-direction results in lengthening of one side from a length of b_y to a length of b_y'. Contraction of the surface in the x-direction results in shortening of one side from a length of a_y to a length of a_y'.

The elongation of the surface in the y-direction and the contraction of the surface in the x-direction can be described by calculating the respective primary strain in the y-direction (ε_{y1}) and secondary strain in the x-direction (ε_{x2}):

$$\varepsilon_{y1} = \frac{b'_y - b_y}{b_y} \qquad \varepsilon_{x2} = \frac{a'_y - a_y}{a_y} \tag{46}$$

These strains are related to the stress in the y-direction through the elastic modulus (E) and Poisson's ratio (ν) by the following relationships:

$$\varepsilon_{y1} = \frac{\sigma_y}{E} \qquad \varepsilon_{x2} = -\nu\varepsilon_{y1} = -\nu\frac{\sigma_y}{E} \tag{47}$$

The total strain in the x-direction (ε_x) and the y-direction (ε_y) can be determined by summing each of the components from equations (33) and (35):

$$\varepsilon_x = \varepsilon_{x1} + \varepsilon_{x2} = \frac{\sigma_x}{E} - \nu\frac{\sigma_y}{E} \tag{48}$$

$$\varepsilon_y = \varepsilon_{y1} + \varepsilon_{y2} = \frac{\sigma_y}{E} - \nu\frac{\sigma_x}{E} \tag{49}$$

For equal biaxial loading of a cubic element the lengths of all sides of the element are equal ($a = b = c$), the areas of all surfaces are equal ($A_x = A_y$), and the force applied in the x-direction is equal to the force applied in the y-direction ($F_x = F_y$). It follows from these equivalencies that the stresses applied in the x-direction is equal to the stress applied in the y-direction as shown in the equation below:

$$\sigma_x = \sigma_y \tag{50}$$

This results in simplification of equations (36) and (37) to the following expressions:

$$\varepsilon_x = \frac{\sigma_x}{E} - \nu\frac{\sigma_y}{E} = \frac{\sigma}{E} - \nu\frac{\sigma}{E} = \frac{\sigma}{E}(1-\nu) \tag{51}$$

$$\varepsilon_y = \frac{\sigma_y}{E} - \nu\frac{\sigma_x}{E} = \frac{\sigma}{E} - \nu\frac{\sigma}{E} = \frac{\sigma}{E}(1-\nu) \tag{52}$$

$$\therefore \varepsilon_x = \varepsilon_y \tag{53}$$

An expression for the modulus can thus be obtained by rearranging terms as shown in the equation below:

$$E = \frac{\sigma}{\varepsilon}(1-\nu) \tag{54}$$

For an incompressible material Poisson's ratio is 0.5 and this expression simplifies to the following:

$$E = \frac{\sigma}{\varepsilon}(1-0.5) = \frac{\sigma}{2\varepsilon} \tag{55}$$

Stress was calculated by dividing the tension determined as described in section 4.1.6 at each data point by the thickness of the sample. The linear infinitesimal strain was determined as described in section 4.1.5. A numerical value for modulus was obtained using the method described in section 4.1.7. It is important to note that this modulus is defined only for biaxial loading and is not comparable to the modulus measured using other conditions such as uniaxial loading.

4.2 Alteration of Scaffold Stiffness by Cell Culture Methods

The utility of the membrane inflation method to model the mechanical properties of tissue engineered cardiac scaffolds immediately after implantation was evaluated. Veritas was used for this study because previous work in this lab (Filipe, McBride, Murphy, & Singh, 2007) has demonstrated that it has a higher ultimate tensile strength than the ECM evaluated in the previous section. It was demonstrated that the strength of Veritas is sufficient to withstand the forces generated in the left ventricle, thus expanding its applicability beyond the narrow use of ECM which is limited to the right ventricle.

It was hypothesized that exposure of Veritas to cell culture conditions would alter the mechanical properties of the scaffold through several possible mechanisms, including deposition of extracellular matrix proteins on the scaffold or enzymatic degradation of the scaffold. In order to assess

the effects which different aspects of cell culture methods may have on scaffold stiffness, the following questions were investigated:

- Question 1: What effect does time in culture media have on scaffold stiffness?
- Question 2: What effect does cell seeding have on scaffold stiffness?
- Question 3: What effect does supplementation of media with ascorbic acid have on scaffold stiffness?

In order to assess the effects which each of these aspects of cell culture have on scaffold stiffness, samples were allocated to the four experimental groups outlined in Table 2.

Table 2: Summary of Experimental Groups

Experimental Group	Group Description	Cell Culture Conditions		
		Time in Culture Media	Cell Seeding	Media Supplementation
Group 1	Veritas Control	None	None	No Media
Group 2	Veritas Unseeded	2, 4, 10 Weeks	None	No Supplementation
Group 3	Veritas + HDF	10 Weeks	Human Dermal Fibroblasts	No Supplementation
Group 4	Veritas + HDF + AA	10 Weeks	Human Dermal Fibroblasts	Ascorbic Acid

The effect which each of the individual aspects of cell culture has on scaffold stiffness was evaluated by making comparisons between the groups as outlined in Table 3.

Table 3: Comparisons between Experimental Groups

Question	Comparison
Question 1: Effect of Time in Culture Mediua	Group 1 vs. Group 2
Question 2: Effect of Cell Seeding	Group 2 vs. Group 3
Question 3: Effect of Media Supplementation	Group 3 vs. Group 4

4.2.1 Scaffold Preparation

Veritas collagen matrix scaffolds (Synovis Surgical Innovations, Saint Paul, MN) were cultured with human dermal fibroblasts in standard media or in media supplemented with 50 µg/mL ascorbic acid (see Appendix A: Determination of Ascorbic Acid Concentration). These were compared to scaffolds incubated in standard media without any cells and to control scaffolds tested directly after removal from the manufacturer's packaging.

The scaffolds were prepared by cutting 2cm x 2cm samples and placing each sample into one well of a 6 well plate. The bottoms of size 114 PTFE O-rings (I.D = 12.7 mm, O.D. = 15.9mm) were coated

with sterile vacuum grease to create a ridge approximately 1mm in height. A vacuum grease coated O-ring was placed onto the center of each sample and pressed down to create a tight seal. Four hundred fifty thousand cells were delivered to each sample in a 400µL volume of cell suspension. The samples were placed in the incubator for four hours to allow the cells to attach before removing the O-rings and transferring the scaffolds to a new 6 well plate and adding 2mL of media to each well. The samples were returned to the incubator and media was changed every 4-5 days. Four of the samples were incubated in Dulbecco's Modified Eagle Medium (DMEM) supplemented with 1% Penicillin/Streptomycin (P/S) and 10% Fetal Bovine Serum. An additional four samples were incubated in the same medium supplemented with 50 µg/mL Ascorbic Acid. Samples were cultured for ten weeks. An incubation time of 10 weeks was selected because an initial pilot study detected minimal changes in mechanical properties after 2 and 4 weeks (See Appendix D).

To elucidate the effect that media alone has on the scaffolds, samples were incubated in DMEM containing 10% DMEM and 1% P/S without any cells. Two samples were removed from culture after two, four, and ten weeks and the mechanical properties were measured.

4.2.2 Scaffold Characterization

At the end of the incubation periods the samples were removed from culture, soaked in deionized water for one hour to lyse the cells, and tested with the membrane inflation method as described previously. Thickness was measured prior to testing using the laser displacement system. Due to the non-linearity of the samples the linear region was defined as the upper 50% of the data points and the slope and intercept were thus calculated over this range. The stiffness and modulus were computed as described in section 4.1.7 above.

Prior to mechanical testing, the samples were subjected to the Alamar Blue stain in order to qualitatively assess the presence of cells on the samples. The Alamar Blue assay measures the ability of cells to reduce the Alamar Blue dye and can thus be used to assess their metabolic activity. The media in each well was replaced with a 1:10 solution of Alamar Blue dye in serum free DMEM and incubated at 37°C for 2 hours. Quantitative analysis was not possible since the scaffold absorbed a significant amount of the dye. Digital images of the samples were taken after the incubation period.

After mechanical testing, the samples were frozen at -80°C and lyophilized. A scalpel was used to divide the samples into two portions. The interior portion was the region of each sample enclosed by the O-ring and on which cells were placed, while the exterior portion was the region of the scaffold outside of the O-ring. The interior and exterior portions of each scaffold were diced into small pieces and each portion was divided into two groups for biochemical analysis.

The percent of scaffold dry weight which is comprised of collagen was determined for each scaffold as well as the amount of collagen which is enzymatically degradable under defined conditions. Total collagen was determined by hydrolyzing a known mass of scaffold and measuring the collagen concentration of the resulting solution using the Hydroxyproline assay. The total mass of collagen in the solution was calculated and divided by the initial sample mass to determine the total collagen percentage. The amount of enzymatically degradable collagen was determined by adding one milliliter of 1mg/mL pepsin in 0.5M acetic acid to each sample and incubating for 5 days on a rocker at 4°C.

Samples were centrifuged at 3,000 g to pellet any undigested material and the supernatant was removed for analysis. The collagen concentration of the supernatant was measured using the Hydroxyproline assay. The total mass of collagen in the supernatant was calculated and divided by the initial sample mass to determine the percentage of the sample which was comprised of acid/pepsin soluble collagen.

The collagen content of the samples was estimated using the Hydroxyproline assay (Ignat'eva, Danilov, Averkiev, Obrezkova, Lunin, & Sobol, 2007). Hydroxyproline is an amino acid unique to connective proteins such as collagen, thus making its identification useful as an estimator of collagen content. Diluted samples are hydrolyzed by exposure to strong acid under high temperature in order to break down the proteins into their component amino acids. The Hydroxyproline molecules are oxidized using Chloramine-T and any excess Chloramine-T is decomposed by perchloric acid. Ehrlich's reagent reacts with the oxidized Hydroxyproline molecules forming a strongly colored solution. The sample extracts were diluted 1:10 in deionized water and broken into their component amino acids by hydrolyzing them in 6N HCl at 110°C for 18 hours. The samples were then neutralized with 1N HCl and 1N NaOH to a pH of 6.8-8.2 and the volumes were brought to 7mL with water. One milliliter aliquots of each sample were transferred to glass tubes for all further reactions. The oxidizing reagent Chloramine-T was added to each tube in 0.5mL aliquots and allowed to sit at room temperature for 20 minutes. One half of a milliliter of 3.15M Perchloric Acid was added for 5 minutes at room temperature and 0.5mL of Ehrlich's Reagent was added for 20 minutes at 60°C to induce color development. The sample tubes were cooled in cold tap water for 5 minutes prior to transferring 200µL aliquots to a 96-well plate and reading the absorbance at 561nm. Absorbance values were converted to collagen concentrations based on a standard curve of acid-soluble bovine collagen.

The glycosaminoglycan (GAG) content of the scaffolds was determined using the Blyscan Glycosaminoglycan assay (UK Biocolor, Ltd.). The Blyscan Assay is a quantitative dye-binding method for the analysis of sulfated proteoglycans and glycosaminoglycans. The dye label used in the assay is 1,9-dimethylmethylene blue and the dye is employed under conditions that produce a specific label for the sulfated polysaccharide component of proteoglycans and/or the protein-free sulfated glycosaminoglycan chains. Chondroitin sulfates (4 and 6 sulfated), keratin sulfates (alkali sensitive and resistant forms), dermatan sulfate (containing iduronic and glucuronic acid), and heparin sulfates (including heparins) can be detected by the Blyscan Assay. Briefly, one-hundred microliter samples of a salt extract (48 hours, 1 M NaCl in 0.05 M Tris-HCl, pH = 7.5) were incubated with the assay dye reagent on a rotation mixer for 30 minutes. The samples were centrifuged for 10 minutes at 10,000 g in order to pellet the bound dye. The dye reagent was replaced with a dissociation reagent and incubated on a rotation mixer for 10 minutes. Samples of the solution were transferred to a 96-well plate and the absorbance at 656nm was recorded using a plate reader. Absorbance values were converted to GAG concentrations based on a standard curve of chondroitin-4-sulfate.

4.3 Statistics

The mean and standard deviation was calculated for each measured parameter. For cases in which multiple measurements were taken on individual samples the standard error of the mean was determined.

Differences between two groups were analyzed using a Student's unpaired t-test assuming unequal variance. If a comparison was being made between more than two groups an ANOVA analysis with a Tukey post-hoc test was used. Significance was established for p-values less than 0.05 in both cases.

Calculation of descriptive statistics, t-tests, and regression analyses were performed using Excel 2010 (Microsoft Corp., Redmond, WA). ANOVA analyses were performed using REvolution R 1.3.0 (REvolution Analytics, Palo Alto, CA).

Chapter 5: Results

5.1 Comparison of *In Vivo* Testing with Membrane Inflation Testing

5.1.1 *In Vivo* Testing: General Results

Examination of the sonomicrometry data showed that each of the three measured cardiac axes varies with time as demonstrated by a representative data set in Figure 14. This demonstrates that the implanted sonomicrometry crystals represent the changes in global cardiac dimensions which occur throughout the cardiac cycle.

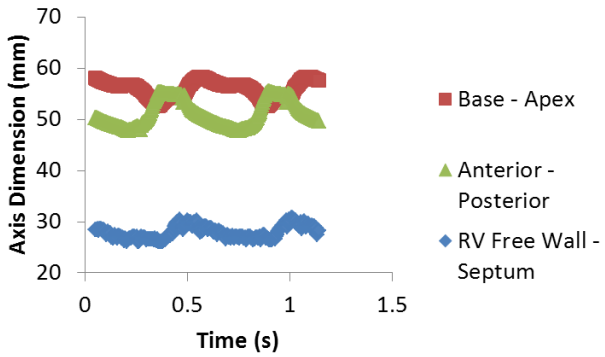

Figure 14: Variation of cardiac axes throughout heartbeat

This observation was reinforced by comparing the maximum and minimum values for each axis as shown in Table 4. The results of a Student's paired t-tests demonstrated that statistically significant differences exist between the maximum and minimum values for each axis. The average variation of each axis from its mean value which occurs as the heart progresses throughout the cardiac cycle is also reported.

Table 4: The maximum, minimum, and mean values of each sonomicrometry axis are reported. The ranges of values which occur during a heartbeat are also given as a percentage of the mean axis values.

Dimension	Maximum Length (mm)	Minimum Length (mm)	Mean Length (mm)	Variation from Mean During Heartbeat (%)
RV Free Wall – Septum (n=8)	32.6 ± 7.2	26.9 ± 6.5	27.3 ± 6.7	16.7 ± 7.4
Anterior – Posterior (n=8)	55.7 ± 6.9	49.5 ± 7.8	56.3 ± 9.2	9.3 ± 5.6
Base – Apex (n=8)	60.8 ± 4.1	55.5 ± 4.4	59.2 ± 4.1	7.4 ± 2.2

In addition to the variation in each of the axes which occurs throughout the cardiac cycle, the average axis lengths also varied between each of the measured heart samples as shown Figure 15.

	Length (mm)	COV (%)
RV Free Wall – Septum (n=8)	27.3 ± 6.7	24.6
Anterior – Posterior (n=8)	56.3 ± 9.2	16.3
Base-Apex (n=8)	59.2 ± 4.1	6.85

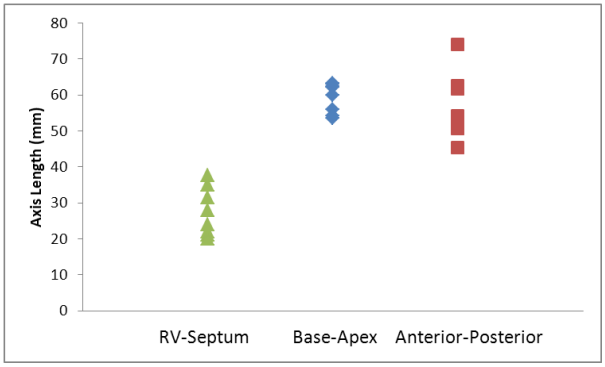

Figure 15: Variation of sonomicrometry axes between hearts

Examples of the work loops obtained for both a Dacron scaffold and an ECM scaffold are shown in the left plot in Figure 16. The corresponding loading portions of these work loops, defined by continuously increasing pressure, are shown in the right plot.

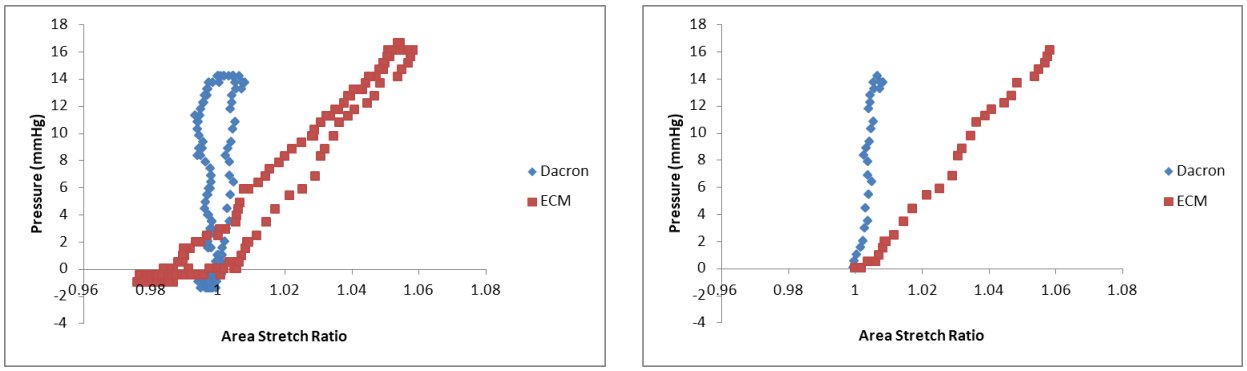

Figure 16: Work loops for ECM and Dacron scaffolds are shown in the plot on the left. The loading portions of these data sets are shown in the plot on the right

The average variation in right ventricular pressure throughout a heartbeat was 17.2 ± 1.8 mmHg. The area stretch ratio at end diastole was 1.004 ± 0.01 for Dacron scaffolds and 1.059 ± 0.04 for ECM scaffolds. No statistically significant difference exists between the materials ($p = 0.07$), however a strong trend of ECM being more extensible than Dacron was observed.

5.1.2 *In Vivo* Testing: Scaffold Loading

The ellipsoid used to model the right ventricle was fairly elongated as evidenced by an inspection of the dimensions of the ellipse formed by taking its cross-section along the major axis. The eccentricity obtained from each heart varied between 0.8 ± 0.05 and 0.9 ± 0.05 as the geometry of the heart changed throughout the cardiac cycle. When the eccentricity has a value of zero, the shape of the ellipse approaches that of a circle while when the eccentricity has a value of one, the shape of the ellipse approaches that of a line segment. The eccentricities measured here thus demonstrate that the ellipse has an elongated shape. This was confirmed by examining the lengths of the semi-major axes and semi-minor axes shown in Table 5.

Table 5: The lengths of the semi-major and semi-minor axes of the ellipse used to model the right ventricle

Dimension	Length
Semi-Major Axis (mm)	26.8 ± 2.2
Semi-Minor Axis (mm)	56.6 ± 5.6

The radii of curvature varied from a minimum value of 49.3 mm to a maximum value of 65.5 mm. The mean and standard deviation for the radius of curvature were 56.6 ± 5.6 mm. The maximum tension at the outermost point of the right ventricular free wall was 395 ± 103 mmHg-mm. The tension and area stretch ratio during diastole are shown for each material in Figure 17.

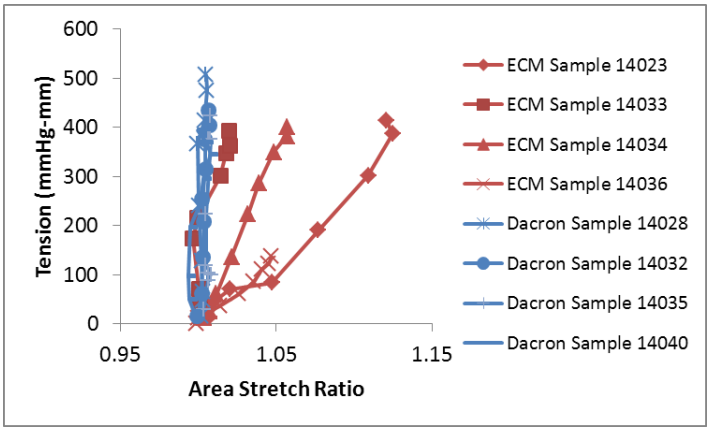

Figure 17: The loading and deformation applied of scaffolds during diastole

5.1.3 Membrane Inflation Testing: General Results

The initial hydrated thickness of the Dacron samples was 0.50 ± 0.03 mm and the thickness of the ECM scaffolds was 0.43 ± 0.01 mm. Average displacements and pressures as well as loading curves for representative samples of Dacron and ECM are shown in Figure 18. A statistically significant difference existed between the displacement at maximum pressure for Dacron and for ECM.

	Dacron (n=3)	ECM (n=3)
Maximum Pressure (mmHg)	200 ± 0.0	200 ± 0.0
Displacement at Maximum Pressure (mm)	0.22 ± 0.05	0.59 ± 0.01

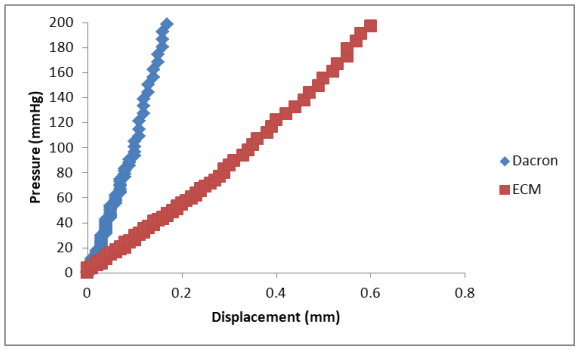

Figure 18: Raw data obtained from membrane inflation testing

5.1.4 Membrane Inflation Testing: Scaffold Deformation

The radius of curvature decreased from infinity for unloaded samples to its minimum value at the maximum pressure of 200mmHg. A statistically significant difference existed between the minimum radius of curvature for Dacron and for ECM ($p<0.05$). Representative plots for ECM and Dacron are shown in Figure 19.

	Dacron (n=3)	ECM (n=3)
Radius of Curvature at 200 mmHg (mm)	63.8 ± 7.9	21.4 ± 0.43

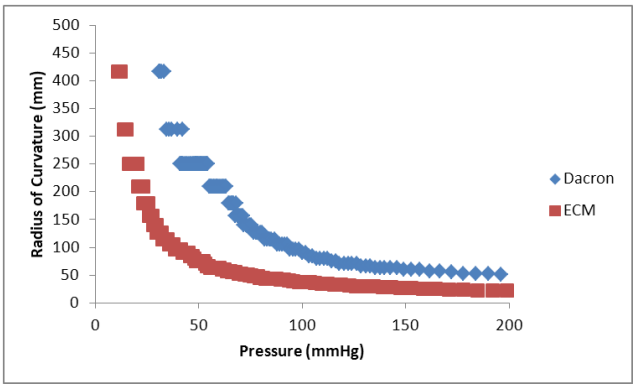

Figure 19: Dependence of radius of curvature on pressure

Figure 20 shows representative plots obtained when area stretch ratio as calculated from the radius of curvature is used to describe sample deformation. The plots are zeroed to account for the removal of the non-linear lower regions of the data-sets. A statistically significant difference existed between the area stretch ratio at a pressure of 200 mmHg for Dacron and for ECM ($p<0.05$).

	Dacron (n=3)	ECM (n=3)
Area Stretch Ratio at 200 mmHg	1.001 ± 0.000	1.013 ± 0.001

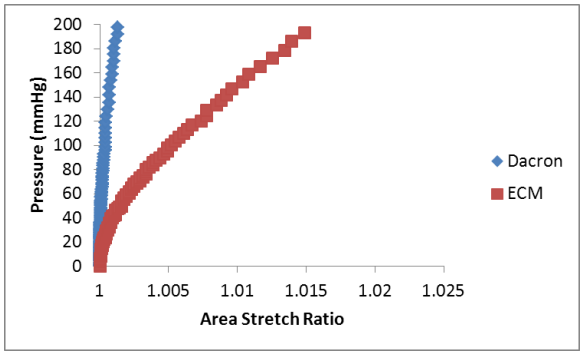

Figure 20: Area stretch ratio for representative Dacron and ECM samples

5.1.5 Membrane Inflation Testing: Scaffold Loading

The center displacement of the deformed samples was used to calculate the radius of curvature, from which the tension was then determined. As shown in Figure 21, it was noted that since the radius of curvature varies inversely with center displacement, as well as with its square, the relationship between the two parameters is highly non-linear at low displacement values.

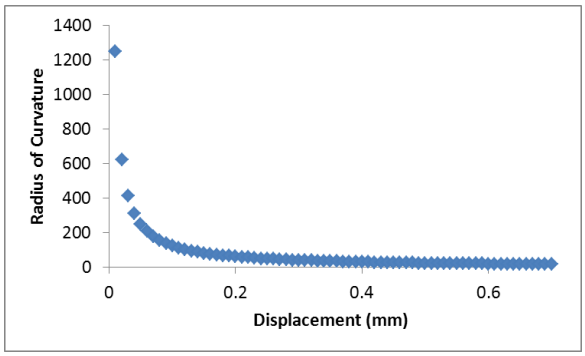

Figure 21: Radius of curvature varies non-linearly with center displacement at low values

The non-linearity of the relationship between center displacement and radius of curvature means that small errors in center displacement will result in large changes in radius of curvature. Calibration of the laser displacement system used to measure center displacement is performed using a micrometer accurate to 2 decimal places (i.e. 0.50 mm). Thus, the percent change in radius of curvature resulting from an error of ± 0.01 mm was examined over the range of center displacement values which were measured. As shown in Figure 22, the percent change in radius of curvature decreases as the center displacement values increase.

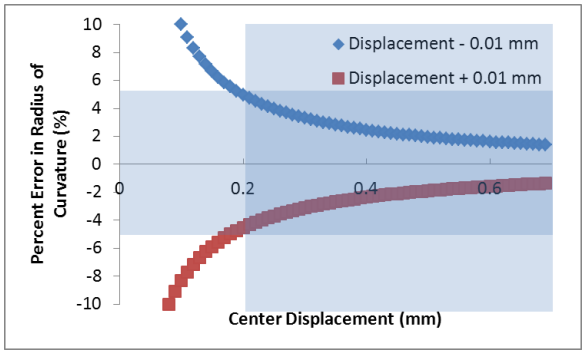

Figure 22: An error of ± 0.01 mm in the center displacement results in less than a 5% change in the calculate radius of curvature for center displacements greater than 0.20 mm. The darkly shaded area contains the region of data which were used to calculate tension.

It was found that the percent change in radius of curvature was less than 5% for center displacements greater than 0.20 mm. Therefore, only radii of curvature calculated from center displacements greater than 0.20 mm were used for the calculation of tension. The tension and area stretch ratio were set to values of 0 and 1 respectively and all subsequent data points were normalized to this baseline. Plots of tension and area stretch are shown for representative samples of Dacron and ECM in Figure 23.

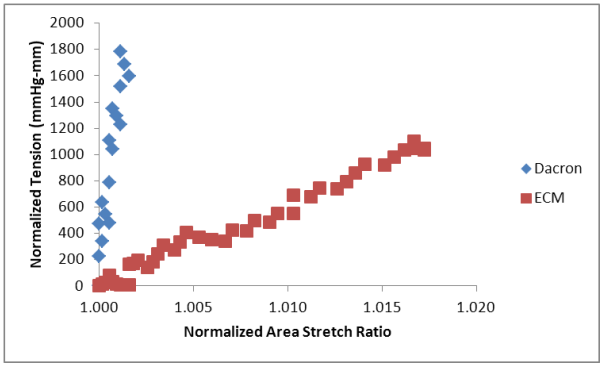

Figure 23: Loading is expressed as tension for a representative Dacron and ECM sample.

The average normalized peak tension and normalized peak area stretch ratio are shown in Table 6 along with non-normalized values for the same parameters. Statistically significant differences existed between the values for Dacron and for ECM for each parameter.

Table 6: Values for peak tensions and peak area stretch ratios in the linear region

	Dacron (n=3)	ECM (n=3)
Normalized Peak Tension	824 ± 130	370 ± 3
Normalized Peak Area Stretch Ratio	1.001 ± 0.001	1.013 ± 0.002
Peak Tension	6,186 ± 690	1,967 ± 203
Peak Area Stretch Ratio	1.002 ± 0.001	1.014 ± 0.001

5.1.6 Comparison of Mechanical Properties of Scaffolds Determined During In Vivo Testing and Membrane Inflation Testing

The analyses performed in the previous sections revealed that membrane inflation testing is able to deform both Dacron and ECM to the same radius of curvature as that which occurs *in vivo*. However, upon examination of the data it is evident that the loading required to deform the samples to this curvature was different *in vitro* than *in vivo*. In order to investigate this further, the tensions and area stretch ratios measured *in* vitro at a typical *in vivo* curvature of 56 mm were determined. These values were compared to the maximum tensions and area stretch ratios measured *in vivo*. The tensions and area stretch ratios measured in each case are shown in Table 7.

Table 7: Comparison of Tensions and Area Stretch Ratios measured *in vitro* and *in vivo*

	Tension (mmHg-mm)		Area Stretch Ratio	
	Dacron	**ECM**	**Dacron**	**ECM**
In Vitro	6,077 ± 800	1,778 ± 71	1.002 ± 0.00	
In Vivo [Note 1]	395 ± 103		1.004 ± 0.01	1.059 ± 0.04

Note 1: Values reported in section 5.1.1 & 5.1.2

It is clear that the tensions developed at the given radius of curvature are substantially higher *in vitro* than *in vivo* and that the area stretch ratios are higher *in vivo* than *in vitro*. Tension is a function of

the pressure applied to a sample and the radius of curvature to which it deforms. Samples tested by membrane inflation require different amounts of pressure to deform them to the specified radius of curvature due to their different stiffnesses. The tension calculated for *in vivo* samples is based on the curvature of the right ventricle and is not dependent on the properties of the different scaffold materials. Thus, different tensions were computed for the different materials *in vitro* while a single tension was determined *in vivo*. Similarly, the area stretch ratio measured for samples tested by membrane inflation is a direct function of the radius of curvature of the samples and thus the same area stretch ratio exists for both materials at the specified radius of curvature. The area stretch ratio measured by HDM *in vivo* is independent of the radius of curvature and thus different values are reported for the different materials.

Despite the differences in tension and area stretch ratios which are noted above, a comparison of the stiffnesses (slopes of the tension-area stretch ratio curves) measured for both materials using both methods is shown in Figure 24.

	Stiffness (10^3 mmHg-mm)	
	Dacron	**ECM**
In Vitro	159 ± 25	31.8 ± 1.2
In Vivo	38.2 ± 8.3	6.79 ± 2.5

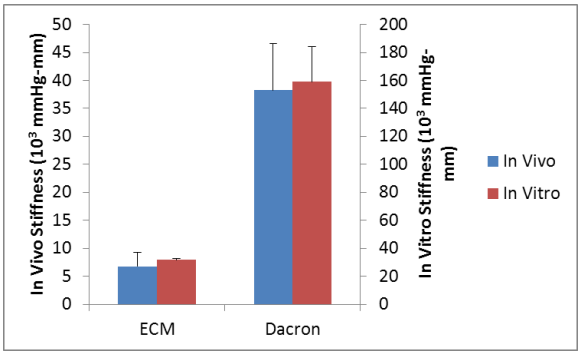

Figure 24: Comparison of stiffness during in vitro and in vivo testing for Dacron and ECM scaffolds

Despite the fact that the *in vitro* stiffness was higher than the *in vivo* stiffness for both materials, the fold-increase in stiffness between ECM and Dacron is similar for both testing methods. A 5.6 ± 3.3 fold increase between the stiffness of ECM and Dacron was found *in vivo* and a fold increase of 5.0 ± 1.0 was found *in vitro*. In addition, the elastic modulus measured by membrane inflation was found to be 22.9 ± 7.8 MPa for the Dacron scaffolds and 6.8 ± 0.2 MPa for the ECM scaffolds.

5.2 Alteration of Scaffold Stiffness by Cell Culture Methods

Having established a method by which the stiffness of cardiac scaffolds can be characterized *in vitro*, a method for altering the stiffness of the scaffolds *in vitro* was examined. The hypothesis that scaffold stiffness can be altered *in vitro* using cell culture techniques was evaluated by investigating the effect of time in cell culture media, the effect of cell seeding, and the effect of supplementing the culture media with ascorbic acid.

Previous animal studies evaluating regenerative cardiac scaffolds have used urinary bladder matrix (UBM) in the right ventricle since the right ventricle has a less severe mechanical loading environment which is ideal for initial studies. However, most myocardial infarctions occur in the left ventricle, and thus in order to be clinically relevant, a scaffold with sufficient mechanical properties

must be used. Veritas collagen matrix, derived from bovine pericardium, is a clinically approved material with superior handling and suturability characteristics to those of UBM. As seen in Figure 25, Veritas has the added advantage that it has a similar mechanical loading profile to that of UBM when measured using membrane inflation testing.

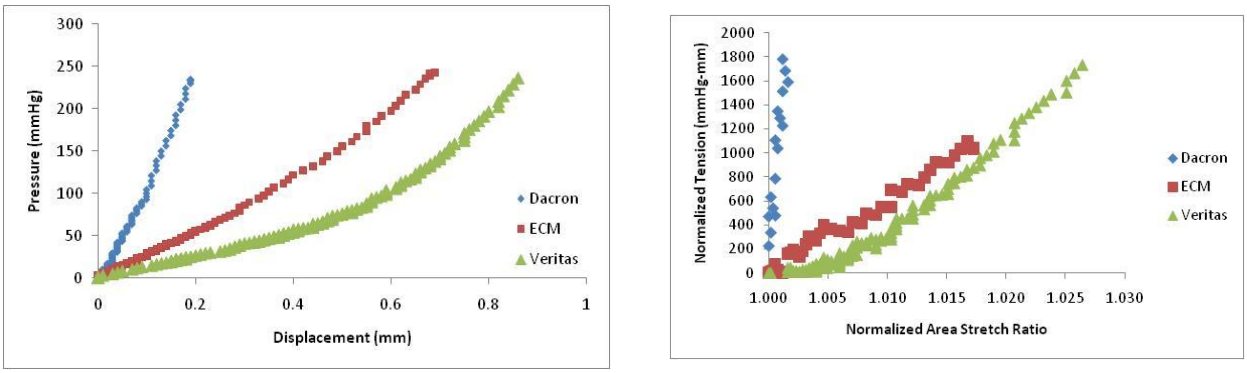

Figure 25: Comparison of representative Veritas samples with representative Dacron and ECM samples. Raw data is shown on the left and Tension vs. Area Stretch ratio is plotted on the right

5.2.1 Scaffold Preparation

Tissue engineered scaffolds were produced by culturing fibroblasts on Veritas with and without ascorbic acid and the mechanical properties were assessed after 10 weeks. All samples were monitored throughout the duration of the culture period and media was changed as directed. The samples were dark purple after Alamar Blue staining, suggesting that cells on the scaffold remain viable at the end of the culture period (see Appendix C for representative image).

5.2.2 Effect of Time in Culture Media on Scaffold Stiffness

A drastic decrease in scaffold stiffness was observed due to the incubation of scaffolds in cell culture media without any cells as shown in Figure 26.

Incubation Time	Stiffness (10^3 mmHg-mm)
0 Weeks (n=2)	47.3 ± 5.7
2 Weeks (n=2)	16.2 ± 2.9
4 Weeks (n=2)	11.2 ± 1.0
10 Weeks (n=2)	0.18 ± 0.1

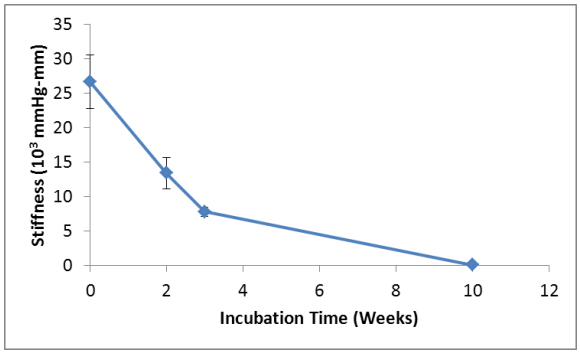

Figure 26: Scaffold stiffness decreases with prolonged time in culture media

This decrease in stiffness due to incubation time in culture media was accompanied by an increase in the thickness of the scaffolds as shown in Figure 27.

Incubation Time	Thickness (mm)
0 Weeks (n=2)	1.35 ± 0.05
2 Weeks (n=2)	0.92 ± 0.00
4 Weeks (n=2)	1.10 ± 0.01
10 Weeks (n=2)	1.63 ± 0.06

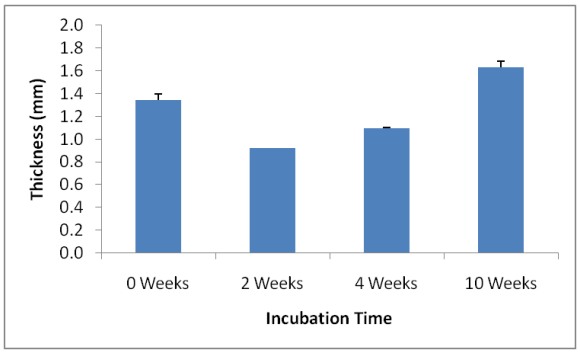

Figure 27: Scaffold thickness has an initial decrease followed by a gradual increase with prolonged time in culture media

It is interesting to note that the thickness of both 2 week and 4 week samples is less than the thickness of 1.35 ± 0.05 measured for control samples. It thus appears that there is an initial decrease in sample thickness followed by a gradual increase, perhaps due to swelling of the material.

The combined effects of decreasing stiffness and increasing thickness were assessed by calculating the Elastic Modulus for each sample as shown in Figure 28. Differences between groups at 2, 4, and 10 weeks were accentuated but the trends remained the same.

Incubation Time	Elastic Modulus (MPa)
0 Weeks (n=2)	3.55 ± 0.52
2 Weeks (n=2)	1.79 ± 0.30
4 Weeks (n=2)	1.04 ± 0.09
10 Weeks (n=2)	0.014 ± 0.01

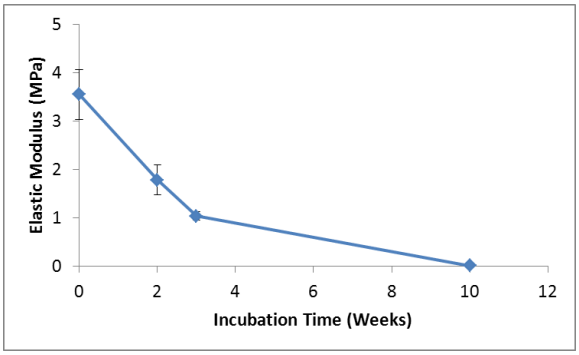

Figure 28: Scaffold elastic modulus decreases with prolonged time in culture media

Only the samples which were incubated in culture media for 10 weeks failed when exposed to pressures of up to 200mmHg. Between 2 weeks and 4 weeks samples had a slight decrease in tension, stress, and radius of curvature while the area stretch ratio increased slightly. The ten week samples had drastically different properties with a lower tension, stress, and radius of curvature and a higher area stretch ratio. The properties of the samples at maximum pressure are shown in Table 8.

Table 8: Mechanical properties of unseeded scaffolds incubated in culture medium for 2, 4, or 12 weeks

Incubation Time	Membrane Inflation Properties at Maximum Pressure				
	Pressure (mmHg)	Tension (mmHg-mm)	Stress (kPa)	Area Stretch Ratio	Radius of Curvature (mm)
0 Weeks (n=2)	200 ± 0	743 ± 121	73.8 ± 14	1.02 ± 0.00	15.8 ± 0.3
2 Weeks (n=2)	200 ± 0	427 ± 81	61.7 ± 12	1.03 ± 0.00	10.6 ± 1.5
4 Weeks (n=2)	200 ± 0	569 ± 91	69.1 ± 11	1.06 ± 0.00	9.2 ± 0.3
10 Weeks (n=2)	53.2 ± 8.6	120 ± 26	9.8 ± 2	1.83 ± 0.05	5.0 ± 0.0

The results presented in this section demonstrate that a substantial deterioration of the scaffold's structural properties occurs when incubated in cell culture media for a prolonged period of time. This loss of structural integrity manifests itself in decreasing stiffness, increasing thickness, and increasing extensibility at failure.

5.2.3 Effect of Cell Seeding on Scaffold Stiffness

The culture of fibroblasts on scaffolds for 10 weeks resulted in a drastic increase in scaffold stiffness as shown in Figure 29. This difference between the groups was statistically significant.

Cell Seeding	Stiffness (10^3 mmHg-mm)
Without Fibroblasts (n=2)	0.188 ± 0.07
With Fibroblasts (n=4)	1.16 ± 0.44

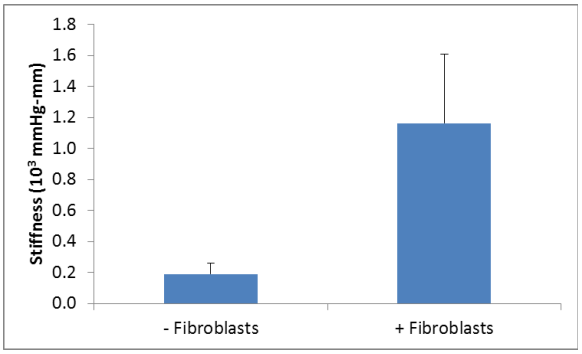

Figure 29: Scaffold stiffness increases after culture with fibroblasts

This increase in stiffness was accompanied by a decrease in thickness. This may be due to swelling of the unseeded scaffolds. Alternately, it may be due to compaction of the seeded scaffolds by the fibroblasts. When stiffness and thickness were combined together and expressed as the elastic modulus, an even more pronounced difference between the groups was observed as shown in Figure 30. The differences between groups were statistically significant for both parameters.

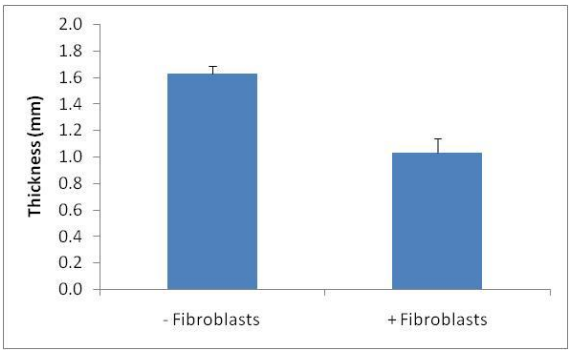

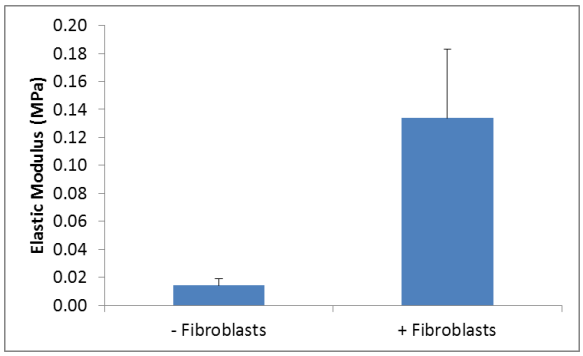

Cell Seeding	Thickness (mm)	Elastic Modulus (MPa)
Without Fibroblasts (n=2)	1.63 ± 0.06	0.014 ± 0.01
With Fibroblasts (n=4)	1.03 ± 0.11	0.134 ± 0.05

Figure 30: Scaffold thickness decreases and scaffold elastic modulus increases after culture with fibroblasts

All scaffolds cultured for 10 weeks failed within the range of pressures that they were exposed to and the failure properties are thus reported here. Pressure at failure, tension at failure, stress at failure, area stretch ratio at failure, and radius of curvature of failure were determined as shown in Table 9.

Table 9: Failure properties of scaffolds seeded with fibroblasts

Cell Seeding	Pressure (mmHg)*	Tension (mmHg-mm)	Stress (kPa)*	Area Stretch Ratio*	Radius of Curvature (mm)
Without Fibroblasts (n=2)	53.2 ± 8.6	120 ± 26	9.7 ± 1.8	1.83 ± 0.05	5.01 ± 0.00
With Fibroblasts (n=4)	106 ± 13	214 ± 35	30.1 ± 5.7	1.23 ± 0.17	6.87 ± 1.23

* Statistically significant differences exist between groups

The failure pressures of scaffolds cultured with fibroblasts were greater than those of the scaffolds in the unseeded group. The failure tensions of the scaffolds cultured with fibroblasts followed a similar trend to the failure pressure. The differences between the thicknesses of the scaffolds were reflected in the failure stresses and more pronounced differences are thus observed between groups.

In addition to characterization of the physical and mechanical properties presented above, changes in the biochemical composition of the scaffolds were also measured. A statistically significant increase in the percentage of sample dry weight comprised of collagen was observed as shown in Figure 31.

Cell Seeding	Total Collagen (%)	Acid/Pepsin Soluble Collagen (%)
Without Fibroblasts (n=2)	54.1 ± 5.1	37.3 ± 9.2
With Fibroblasts (n=4)	83.2 ± 5.1	40.8 ± 4.7

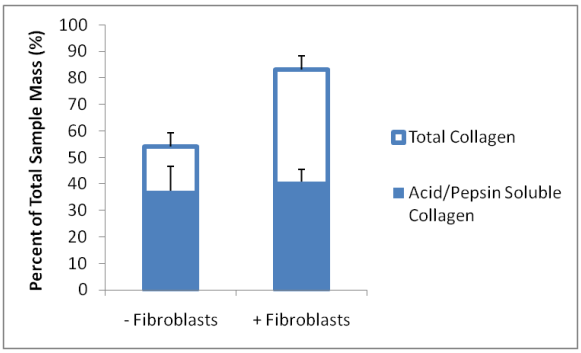

Figure 31: The percentage of sample mass comprised of collagen increases after culture with fibroblasts

The scaffolds cultured with fibroblasts have increased total collagen over the unseeded scaffolds. This is likely due to deposition of collagen by the fibroblasts or to degradation of other non-collagenous proteins. It may also be that the presence of fibroblasts on the scaffolds inhibits a process of collagen degradation which may occur for the unseeded scaffolds.

The changes in total collagen and acid/pepsin soluble collagen can also be expressed by calculating the ratio of acid/pepsin soluble collagen to total collagen. For scaffolds with higher ratios, more of the total collagen is soluble under the enzymatic conditions to which the scaffolds were subjected. As shown in Figure 32, the ratio of acid/pepsin soluble collagen to total collagen decreases, although not to a statistically significant degree, after culture with fibroblasts.

Cell Seeding	Ratio of Acid/Pepsin Soluble Collagen to Total Collagen
Without Fibroblasts (n=2)	0.71 ± 0.24
With Fibroblasts (n=4)	0.49 ± 0.13

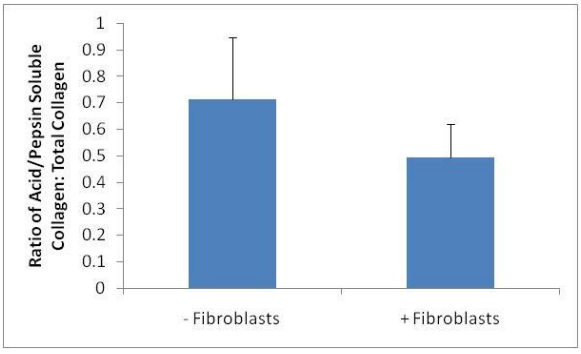

Figure 32: A substantial, although not statistically significant, decrease in the ratio of acid/pepsin soluble collagen to total collagen occurs after culture with fibroblasts

It was hypothesized that one of the potential mechanisms by which scaffold stiffness is altered when seeded with cells is that production of extracellular matrix by the cells alters the scaffold's structure. In order to gain insight into the deposition of extracellular matrix proteins other than collagen, the amount of sulfated glycosaminoglycans (GAG) in the scaffolds with and without fibroblasts was measured. As shown in Figure 33, a statistically significant increase in GAG content occurs in scaffolds after they are cultured with fibroblasts.

Cell Seeding	GAG (%)
Without Fibroblasts (n=2)	0.061 ± 0.02
With Fibroblasts (n=4)	0.236 ± 0.03

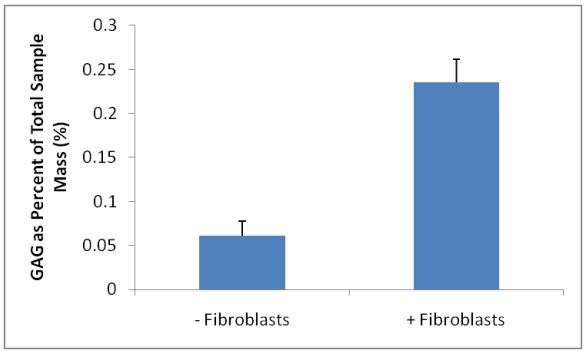

Figure 33: Sulfated glycosaminoglycan content of scaffolds increases after culture with fibroblasts

5.2.4 Effect of Media Supplementation on Scaffold Stiffness

The addition of ascorbic acid to the culture media in which fibroblasts seeded scaffolds were cultured resulted in a slight, although not statistically significant (p = 0.13), drop in scaffold stiffness as shown in Figure 34.

Media Supplementation	Stiffness (10^3 mmHg-mm)
Without Ascorbic Acid (n=4)	1.16 ± 0.44
With Ascorbic Acid (n=4)	0.34 ± 0.13

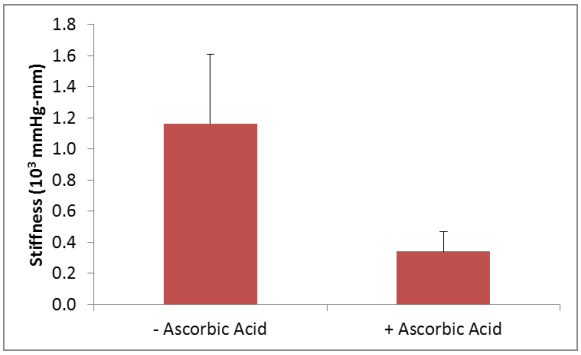

Figure 34: The addition of ascorbic acid to the media during culture of fibroblasts on scaffolds had no statistically significant effect on scaffold stiffness

The addition of ascorbic acid to culture media also resulted in an increase in scaffold thickness which was nearly statistically significant (p= 0.09), along with a statistically significant decrease in elastic modulus. These results are shown in Figure 35.

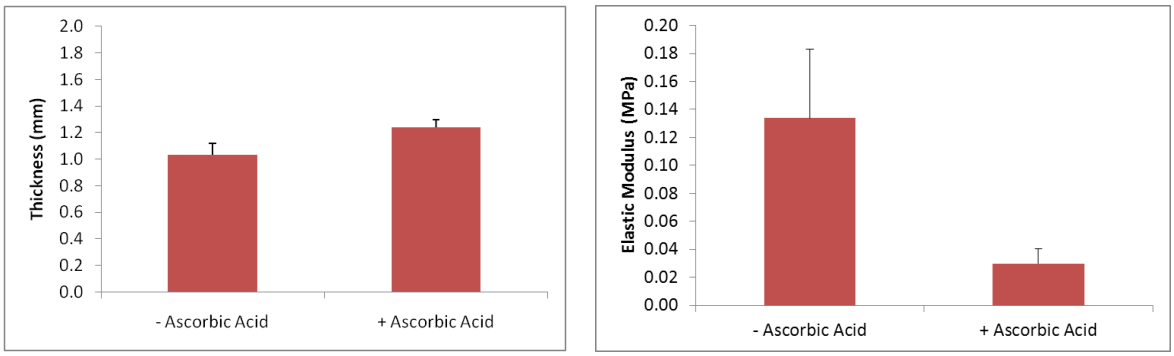

Media Supplementation	Thickness (mm)	Elastic Modulus (MPa)
Without Ascorbic Acid (n=4)	1.03 ± 0.11	0.134 ± 0.05
With Ascorbic Acid (n=4)	1.24 ± 0.08	0.030 ± 0.01

Figure 35: Media supplementation with ascorbic acid results in an increase in thickness and a decrease in elastic modulus

No statistically significant differences were found due to supplementation of the media with ascorbic acid for any of the failure properties shown in Table 10.

Table 10: Supplementation of culture media with ascorbic acid does not result in statistically significant changes in failure properties

Media Supplementation	Pressure (mmHg)	Tension (mmHg-mm)	Stress (kPa)	Area Stretch Ratio	Radius of Curvature (mm)
Without Ascorbic Acid (n=4)	107 ± 13	214 ± 35	30.1 ± 5.7	1.23 ± 0.17	6.87 ± 1.23
With Ascorbic Acid (n=4)	89 ± 30	152 ± 72	15.8 ± 7.0	1.51 ± 0.12	5.37 ± 0.23

Supplementation of culture media with ascorbic acid had no statistically significant effect on the total collagen in the scaffolds. However, a statistically significant decrease in the amount of acid/pepsin soluble collagen was observed as shown in Figure 36.

Media Supplementation	Total Collagen (%)	Acid/Pepsin Soluble Collagen (%)
Without Ascorbic Acid (n=4)	81.2 ± 5.1	40.8 ± 4.7
With Ascorbic Acid (n=4)	67.5 ± 7.3	21.1 ± 3.3

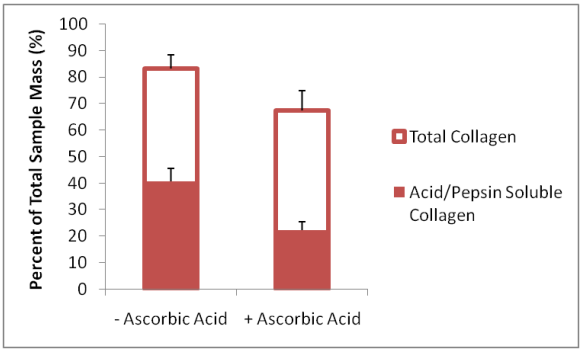

Figure 36: Supplementation of culture media with ascorbic acid results in a decrease in acid/pepsin soluble collagen but not in total collagen

The addition of ascorbic acid to culture media resulted in a substantial, although not statistically significant (p=0.08) decrease in the amount of total collagen which is comprised of acid/pepsin soluble collagen. Results are shown in Figure 37.

Media Supplementation	Ratio of Acid/Pepsin Soluble Collagen to Total Collagen
Without Ascorbic Acid (n=4)	0.493 ± 0.127
With Ascorbic Acid (n=4)	0.329 ± 0.081

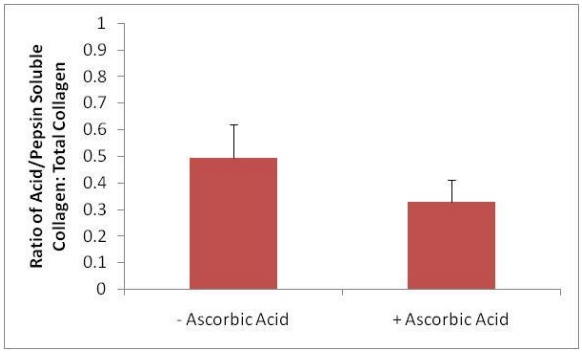

Figure 37: Supplementation of culture media with ascorbic

Supplementation of culture media with ascorbic acid had no statistically significant effect on the amount of GAG in the scaffolds as shown in Figure 38.

Media Supplementation	GAG Content (%)
Without Ascorbic Acid (n=4)	0.236 ± 0.03
With Ascorbic Acid (n=4)	0.206 ± 0.03

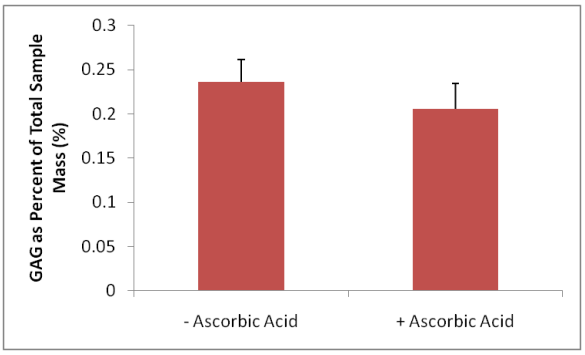

Figure 38: Supplementation of culture media with ascorbic acid does not result in a statistically significant change in GAG content

5.2.5 Correlations between Mechanical Properties and Collagen

In order to gain additional insight into the relationship between changes in scaffold biochemistry and mechanical properties, further analysis of scaffolds cultured for 10 weeks with and without fibroblasts and ascorbic acid was performed. Strong relationships were found to exist between the percentage of acid/pepsin soluble collagen and both total collagen and the ratio of acid/pepsin soluble collagen to total collagen. The correlation between total collagen and acid/pepsin soluble collagen was statistically significant and the correlation between the ratio of acid/pepsin soluble collagen to total collagen and acid/pepsin soluble collagen was nearly significant (p=0.07). These correlations are shown in Figure 39.

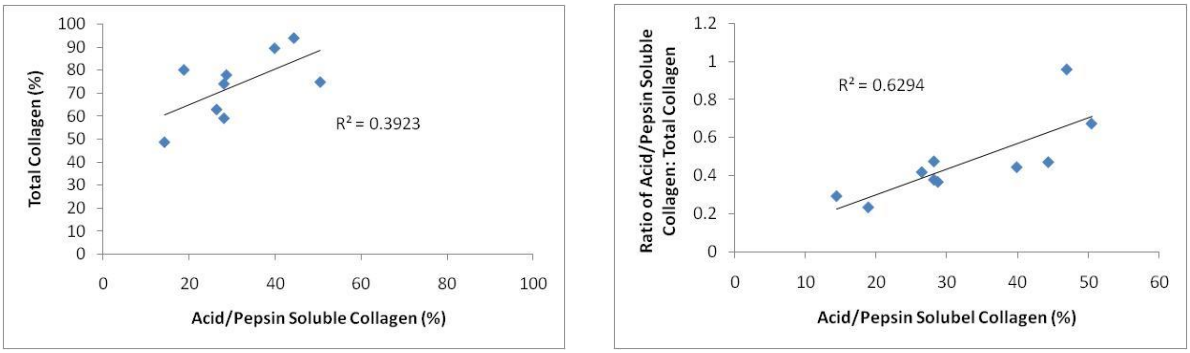

Figure 39: Total collagen percentage is correlated with the percentage of acid/pepsin soluble collagen and with the ratio of acid/pepsin collagen: total collagen

If a decrease in total collagen were a result of similar decreases in acid/pepsin soluble collagen and in acid/pepsin insoluble collagen then the ratio of these two quantities would be expected to be constant for any percentage of total collagen. The positive correlation which the percentage of acid/pepsin soluble collagen has with both the percentage of total collagen and the ratio of acid/pepsin soluble collagen to total collagen suggests that the decrease in total collagen may be due to a decrease in acid/pepsin soluble collagen. Thus, scaffolds with a lower percentage of total collagen have lower percentages of acid/pepsin soluble collagen. In addition, the acid/pepsin soluble collagen which is present in these scaffolds with low percentages of total collagen accounts for a smaller fraction of the total collagen.

The correlation of the mechanical parameters of cell-seeded scaffolds with collagen was also investigated. The correlation coefficient was calculated between the mechanical properties and total collagen, acid/pepsin soluble collagen, and the ratio between the two. Overall the trends observed were weak due to the large spread in data and the presence of outliers. The highest correlation coefficients were observed for thickness, stress at failure, area stretch ratio at failure, and radius of curvature at failure. Since the correlation coefficients were low for tension it is likely that the relatively high correlation coefficients for stress are a result of its dependence on thickness.

As shown in Figure 40 a statistically significant inverse correlation between thickness and total collagen was observed. A week correlation ($p=0.29$) was observed between thickness and the ratio of acid/pepsin soluble collagen to total collagen and no correlation ($p=0.94$) was observed between thickness and the percentage of acid/pepsin soluble collagen.

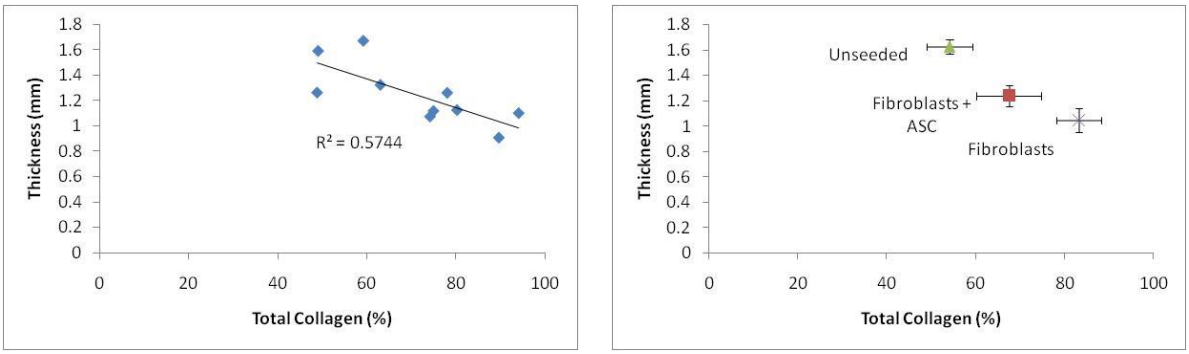

Figure 40: Relationship between thickness and total collagen for each group of tissue engineered scaffolds

Although a strong correlation between stiffness and collagen content was not observed, when elastic modulus was computed for the samples a moderate correlation was found. This is likely due to the fact that the elastic modulus incorporates the thickness of the samples and thickness has already been shown to vary strongly with total collagen. The correlation between elastic modulus and total collagen is shown in Figure 41.

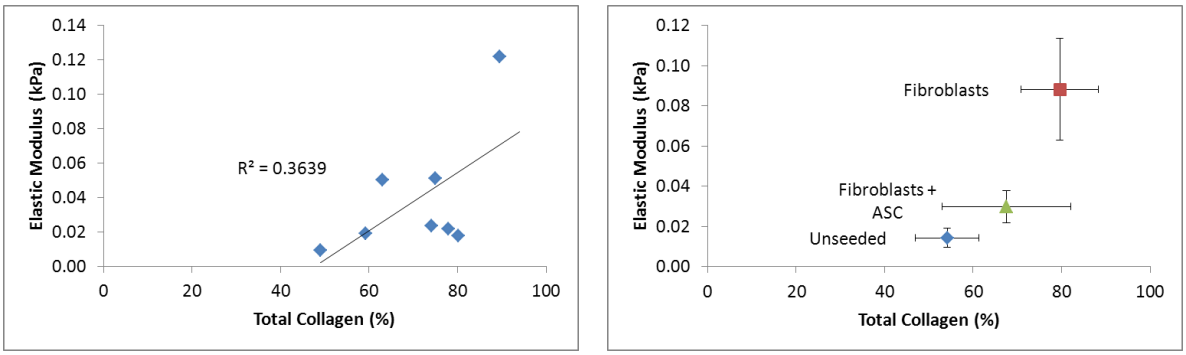

Figure 41: Elastic modulus is strongly correlated with total collagen

In addition to its effect on the structural property of thickness and the sub-failure property of elastic modulus, collagen also has an effect on the extensibility of the scaffolds at failure. A statistically significant correlation was found between the area stretch ratio at failure and the ratio of acid/pepsin soluble collagen to total collagen as shown in Figure 42.

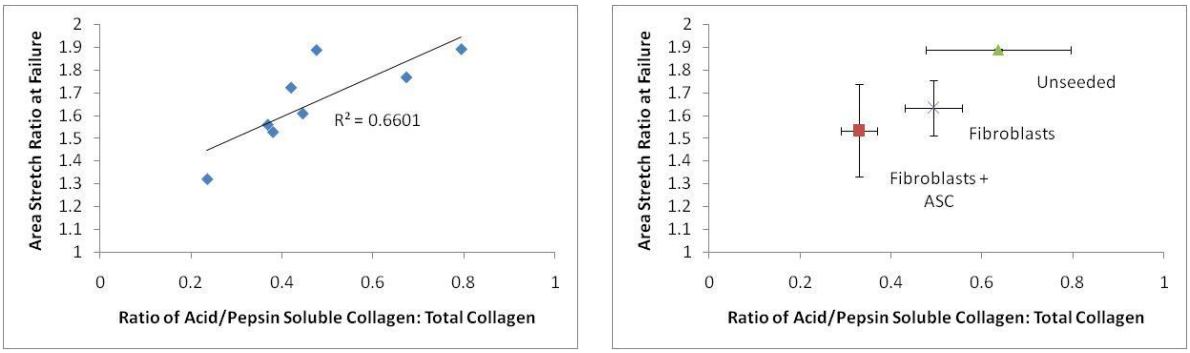

Figure 42: Area stretch ratio at failure is correlated the ratio between of acid/pepsin soluble collagen to total collagen

Area stretch ratio at failure has a negative correlation with total collagen and a positive correlation with acid/pepsin soluble collagen (data not shown). When the correlation with the ratio between these two components is considered a strong positive trend is observed. This infers that with higher amounts of acid/pepsin soluble collagen the area stretch ratio at failure is greater. Another way of expressing this is that higher levels of insoluble collagen result in scaffolds which are less extensible and will fail at lower area stretch ratios.

Weak correlations were found between each of the collagen components and stiffness, stress at failure, and tension at failure. Results are given in Appendix B.

Chapter 6: Discussion

The stiffness of cardiac scaffolds is thought to be an important property which contributes to the process of tissue regeneration. In this project an *in vitro* method for characterizing the stiffness of cardiac scaffolds was shown to yield similar results to those obtained when the same materials are measured *in vivo*. This method was used to assess the effects which cell culture has on the stiffness of a biological membrane scaffold. The ability to characterize and alter the stiffness of cardiac scaffolds will play an important role in the development of scaffolds with improved mechanical properties. This chapter will discuss the significance of these results as well as factors which affect their interpretation.

6.1 Stiffness

A myocardial infarction is a traumatic event which can be fatal if left untreated. Surgical ventricular restoration (SVR) is a promising therapy which may not only reduce the risk of fatality, but also result in regeneration of tissue in the infarcted region. Regeneration is a complex process involving a host of factors. One set of factors is the structural and biochemical composition of the scaffold used to replace the infarcted tissue. Repopulation of the scaffold with functional cardiac cells requires that the material's structure be such that cells can migrate into it and that the biochemical composition be such that the cells will have an affinity to it. An additional factor which impacts the process of regeneration is the stiffness of the scaffold material. The scaffold's stiffness impacts both the development of the cells as well as their ability to eventually deform the scaffold. While optimization of scaffold stiffness alone will not ensure that regeneration occurs, it is an important component of this complex process. The exact range of scaffold stiffness values which is ideal for regeneration has not been identified, and the aim of this study is to provide a basis from which these types of studies can be conducted.

Stiffness is a description of how the loading and deformation of a material are related to each other, and can be expressed as either an intrinsic or a structural stiffness. The intrinsic stiffness of a material describes the stress developed in an infinitesimal portion of a sample when a given strain is applied under simple conditions. The structural stiffness of a material describes the stress developed in a sample of particular size and shape when a given strain is applied under a specified set of conditions. The structural stiffness is a useful parameter since it is an accurate description of exactly what is occurring based on the measurements that have been taken. The disadvantage of the structural stiffness is that the value obtained cannot be compared to similar values obtained from different experimental configurations. The intrinsic stiffness is a useful parameter in that it describes the absolute properties of a material irrespective of the manner in which it is tested. The structural stiffness was calculated for samples in this study by dividing the tension in the samples by their area stretch ratio. It was hypothesized that because of the similar geometric conditions and analysis method between the *in vivo* and membrane inflation experimental conditions the structural stiffness could be compared between the two methods. The intrinsic stiffness was also determined by calculating the Elastic Modulus for samples so that the values could be compared to those reported in the literature.

It should be noted that the equibiaxial stiffnesses calculated in this study are not equivalent to stiffnesses reported from uniaxial testing. A rectangular sample in the x-y plane loaded in the x-direction

will undergo deformation in the y-direction as described by Poisson's ratio, due only to the load in the x-direction. This is in contrast to the same sample to which equal loads are applied in the x and y directions simultaneously. In this case, the deformation in the y-direction will be due to the loading in both the x and y directions. The same argument holds true for the stresses, and it is thus clear that although the expressions for uniaxial and equibiaxial stiffness are mathematically equivalent, the stress and strain in each of these expressions are defined differently. The intrinsic stiffness calculated in this study can thus only be compared to intrinsic stiffnesses in the literature which have been obtained under equibiaxial loading conditions.

Stiffness was calculated for samples tested in this study by assuming that the materials were homogeneous, transversely isotropic, and linearly elastic. While it is apparent that local inhomogeneity does exist within each of the materials, it was assumed that these local inconsistencies average with each other to produce a material which can be considered to be homogeneous. The assumption of transverse isotropy implies that the material properties of the samples were the same in all directions in the plane. It is clear from the gross morphology of the samples that distinct fiber populations exist. However, it was assumed that although local anisotropies may exist, these properties average out to produce a global isotropy. For a synthetic woven material such as Dacron, two orthogonal fiber populations exist and the material can be considered be orthogonally isotropic. Orthogonal isotropy is a special case of transverse isotropy which, under equibiaxial loading, can be treated equivalently. The stress-strain relationship for the Dacron and urinary bladder matrix (UBM) tested in this study was observed to be linear. The stress-strain relationship was found to be consistent over the course of ten repeated cycles, thus verifying the assumption that the materials were elastic. The stress-strain relationships for control Veritas samples was slightly non-linear over the full range of stress and strain which were measured. However, analysis was only performed on the upper 50% of each data set, where the curves were linear. Veritas samples which had been exposed to cell culture conditions had highly non-linear stress-strain relationships. Again, analysis was only performed on the upper 50% of each data set where the stress-strain relationship was linear. Due to the failure of these samples cyclic loading could not be performed and the assumption of elasticity could not be confirmed.

6.2 Advantages and Disadvantages of Membrane Inflation as a Mechanical Testing Method

Membrane inflation testing was used to characterize the stiffnesses of the scaffolds investigated in this study. Membrane inflation testing is an ideal characterization method because it requires minimal manipulation of the scaffolds during sample preparation, and because of the ideal size and shape requirements.

One of the primary advantages of membrane inflation testing is that minimal manipulation is required in order to prepare samples for testing. The only manipulation of the sample which occurs is the clamping of the sample around the edges of the pressure chamber to secure it in place. While failure at the clamp could occur for fragile samples, the failure of samples tested in this study occurred at the center of the sample. This failure mode demonstrated that any clamp induced changes to the sample structure were small in comparison to the tension in the sample generated during sample loading. The

minimal sample manipulation required for membrane inflation testing is in contrast to that required to prepare samples for testing using uniaxial or biaxial devices. In order to avoid stress concentrations due to gripping, uniaxial test samples are cut into “dog bone” shapes. Cutting the sample into a dog bone shape is likely to disturb the native fiber architecture of the sample, thus reducing the sensitivity of this method to slight changes in the structure of the material being tested. Substantial manipulation is also required when preparing samples for analysis using a biaxial testing device. Samples are often secured to biaxial test devices by placing multiple hooks into each of the four sides of the rectangular sample. This time consuming process requires substantial sample handling which may result in crushing of fibers and an alteration of the existing fluid retention properties.

The size and shape required for samples to be tested by membrane inflation testing makes it an ideal method for testing scaffolds to which cell culture manipulations have been applied. As demonstrated in this study, scaffolds cultured with cells in a well of a 6-well plate are sufficiently large to test via membrane inflation testing. The ability to prepare samples on a size scale which is standard for cell culture provides for straightforward and streamlined sample production. The relatively small size of the samples also means that little of the source material is wasted. This is in contrast to the preparation of samples for uniaxial testing which results in substantial waste of source material as the “dog bone” shape is cut out.

Like any test method, membrane inflation testing also has several limitations and disadvantages. One of the most substantial limitations of the membrane inflation method used in this study is that it is not well suited for testing samples which are not transversely isotropic. The displacement of the center of the scaffold was measured and used to estimate strain under the assumption that the material was transversely isotropic and would thus deform to form a spherical cap. If the material were not transversely isotropic, the sample would deform to an oblong shape and other methods would be required in order to determine the strain of the material. One approach which has been used is to measure the deformation of the scaffold by arranging cameras around the sample and acquiring images of the sample’s cross-section while it is inflated (Marra, Kennedy, Kinkaid, & Fillinger, 2006). Image processing could then be used to determine the two perpendicular radii of curvature which describe the curved surface of the inflated sample. Similar methods have been used by other researchers to verify that the samples which they were testing were indeed transversely isotropic (Billiar, Throm, & Frey, 2005) (Slifka, Drexler, Wright, & Shandas, 2006). The possibility that anisotropy leads to the measurement of incorrect strains during membrane inflation testing could be evaluated by simultaneously measuring strain using the standard laser displacement method and HDM.

Another disadvantage of the membrane inflation method used in this study is that it is not ideal for measuring the failure properties of samples. The pressure transducer is only rated for pressures up to 200 mmHg. Many of the un-manipulated or lightly manipulated scaffolds did not fail at this pressure and thus their failure properties could not be determined. To overcome this issue the force transducer could be replaced with one which was rate for higher pressures or a pressure chamber with a larger diameter could be used so that higher radii of curvature could be achieved. However, increasing the pressure chamber diameter would necessitate the use of larger samples which would negate one of the primary advantages of membrane inflation testing. Another approach would be to use uniaxial tensile

testing to characterize the failure properties of the samples. Samples for uniaxial tensile testing are cut to a “dog bone” shape to create a well-defined stress concentration where sample failure will occur.

A final drawback of membrane inflation testing is that it is not ideal for measuring stiff samples since a minimum level of displacement is required to accurately determine sample deformation. The non-linear dependency of the radius of curvature on center displacement at low displacement values was noted in this study. The resulting non-linearity of the radius of curvature manifested itself in non-linear behavior of tension and area stretch ratio at low center displacements. The significance of these parameters in non-linear regions is difficult to assess since small differences in the input (center displacement) result in drastic differences in outputs (radius of curvature, tension, and area stretch ratio). To overcome this, only data outside the non-linear region was used for analysis. This approach has the limitation that for stiff samples which may not have center displacements significantly higher than the cutoff value 0f 0.2 mm, the number of values in the data set is limited. However, the scaffolds tested in this study had sufficient deformations to allow full analysis.

6.3 Comparison of Structural Stiffnesses Obtained *In Vivo* and from Membrane Inflation Testing

In addition to the general considerations discussed in the preceding section, membrane inflation testing was also used because it was observed that the loading and deformation conditions were similar to that of a scaffold implanted into the ventricular wall. Like scaffolds subjected to membrane inflation testing, the ventricular wall is often modeled as a pressure vessel in which pressure is applied to the interior of a curved membrane, resulting in deformation of the membrane and tension in the membrane wall. Based on these assumptions of similar modes of loading and deformation between membrane inflation testing and *in vivo* measurements, it was hypothesized that the structural stiffnesses calculated in each case could be compared with each other and would have similar values.

The loading and deformation occurring *in vivo* was calculated by utilizing a modified form of the shell subtraction model in which the left ventricle was considered to be a sphere and the right ventricle was considered to be half an ellipsoid attached to its side. Because the left ventricle was modeled as a sphere, the right ventricle could be modeled as half of a prolate ellipsoid, that is, an ellipsoid with a circular base. Due to the symmetry of this ellipsoid, the loading at the apex of the ellipsoid was equibiaxial, as was the loading of scaffolds tested using membrane inflation testing. At points other than the apex of the ellipse, the loading was no longer equibiaxial, with two perpendicular tensions corresponding to two perpendicular radii of curvature at each point. The tension increased as the distance from the ellipsoid apex increased since the radius of curvature is larger at points closer to the base of the ellipsoid. At points for which two tensions exist, calculation of the structural stiffness would be challenging in that the area stretch ratio would need to be deconstructed into two separate stretch ratios corresponding to each of the tensions. The HDM images would need to be reexamined and a point on the images corresponding to the apex of the right ventricle would need to be identified. A coordinate transformation could then be performed to align the stretch ratio axes with the directions of the tensions. Since the exact location of the scaffolds in the right ventricular free wall was not readily

available, it was assumed in this analysis that they were implanted at the apex of the ellipsoid used to model the right ventricle.

The structural stiffness used to describe the loading and deformation of the scaffolds tested *in vivo* and by membrane inflation testing was defined as the tension in the scaffolds divided by the area stretch ratio of the scaffolds. Tension was used to describe the loading in the samples because under both testing conditions the mode of loading and deformation was considered to be that of a pressure vessel and loading was estimated using the law of Laplace. Tension was not converted to stress because the thickness of the individual samples used in each animal was not known. Area stretch ratio was used to describe the deformation of the samples since the assumption of equibiaxial loading negated the need to include directionality in the description of deformation. This structural stiffness is distinct from the intrinsic stiffness which was calculated based on the stress, strain, and Poisson's ratio of the samples.

One of the primary assumptions upon which the comparison between *in vivo* and membrane inflation measurements is made is that equibiaxial loading occurs in both testing scenarios. Because of the symmetrical clamping of the sample and the uniform application of pressure during membrane inflation testing, the loading in a homogeneous, transversely isotropic sample should be equibiaxial. Deviation from equibiaxial loading will only occur if the scaffold material is not truly homogeneous and transversely isotropic. The state of equibiaxial loading for *in vivo* samples is dependent not only on the material properties of the scaffold material, but also those of the right ventricle. It is likely that the assumption of homogeneity and transverse isotropy are less accurate for the right ventricular tissue than for the scaffold samples. Well defined bands of muscle fibers are known to exist in the heart tissue, likely leading to uneven deformation and thus an uneven load distribution. An uneven loading distribution in the heart would mean that the loading applied to the implanted scaffold would not be equibiaxial. Evidence of this was found when examining the area stretch ratios measured by HDM. When the area stretch ratio was deconstructed into two orthogonal stretch ratios, different deformations in different directions were observed. The lack of equibiaxial deformation *in vivo* implies that either the cardiac tissue was not transversely isotropic, and thus loading was not equibiaxial, or that the scaffold materials were not transversely isotropic.

Despite the similar modes of loading and deformation which were hypothesized to exist between the two methods, differences in the test methods also existed. These differences likely contributed to the larger deformation and lower loading which were measured *in vivo*. One difference between the methods which may have led to differences in area stretch ratio is that the boundaries of samples tested *In vivo* are not fixed as they are when tested *In vitro*. Scaffolds implanted into the heart are sutured to cardiac tissue which relaxes during systole and stretches as the chamber fills with blood. It is possible that during systole the scaffolds are "compressed" on themselves and thus the area stretch ratio measured during diastole is partially measuring deformation of the scaffold as it returns to a loaded state.

Another difference between the methods is that scaffolds measured by membrane inflation were flat (infinite radius of curvature) in their unloaded state while scaffolds implanted *in vivo* were assumed to take on the radius of curvature of the right ventricle in their unloaded state. The higher tensions observed for samples tested using membrane inflation may be due to the fact that significant loading was required to deform the scaffolds to radii of curvature similar to those which occur *in vivo*. The assumption that scaffolds implanted *in vivo* take on the radius of curvature of the right ventricle is based on a further assumption that the stiffness of the scaffolds is the same as the stiffness of the right ventricle. Differences between the stiffness of the implanted scaffold and that of the right ventricle would result in local radius of curvature for the scaffold which was different than that of the right ventricle. A complex loading scenario would thus exist in which the scaffolds were loaded at their edges with the tension that exists in the right ventricle and would be loaded as a curved membrane by the pressure within the right ventricle. If the scaffolds were stiffer than the right ventricle, the local radius of curvature would be higher than that of the right ventricle and the tension would thus be greater than that of the right ventricle. If the implanted material were less stiff, the local radius of curvature would be lower than that of the right ventricle and the tension would thus be less than that of the right ventricle. This is illustrated in Figure 43.

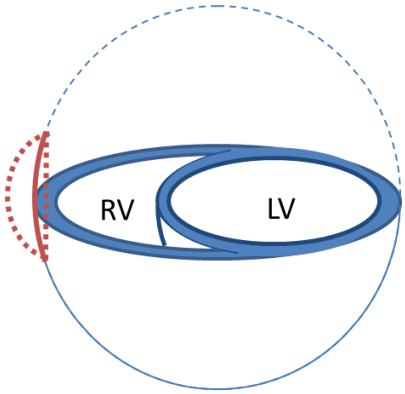

Figure 43: It was assumed that the radius of curvature of the implanted scaffolds was the same as that estimated for the right ventricle (solid red line). If the stiffness of the implanted scaffold were different than that of the right ventricle the radius of curvature would be higher or lower than that of the right ventricle (dashed red lines).

Regeneration of cardiac tissue after a myocardial infarction is a complex process impacted by a multitude of different factors. Replacement of the infarcted tissue with a scaffold may be a treatment approach which facilitates regeneration by supporting the migration of cardiac cells onto the scaffold. The stiffness of the scaffold influences the phenotype into which the cells migrating onto the scaffold will develop as well as the efficiency with which they are then able to deform the scaffold. The ability to characterize the stiffness of the scaffold is thus an important tool in the process of seeking to identify the exact range of stiffnesses which leads to optimal regeneration. As mentioned already, “stiffness” can be defined in a number of different ways. The intrinsic stiffness defines the deformation conditions which develop when a material is subjected to a simple, defined set of loading conditions. The loading conditions to which a material is exposed in most applications are much more complicated than the loading conditions for which the intrinsic stiffness is defined. The intrinsic stiffness is thus no longer an exact description of the relationship between sample loading and deformation. The shortcomings of the

intrinsic stiffness can be addressed by defining the loading and deformation conditions to which the material is actually exposed as accurately as possible. The structural stiffness defines the relationship between these loading and deformation measurements, and reflects how these parameters are associated with each other under the conditions specific to the application in which they are used. The structural stiffness of cardiac scaffolds implanted into the canine right ventricle was determined in this study by directly measuring deformation of the implanted scaffold using HDM, and estimating the loading conditions by modeling the right ventricle as half an ellipsoid and applying the law of Laplace to determine tension. It was noted that samples tested *in vitro* by membrane inflation are deformed to a curved membrane in a similar manner to that which occurs in the geometric model of the right ventricle. Due to the similarities in the loading and deformation conditions which exist for scaffolds implanted *in vivo* and tested by *membrane inflation* it was hypothesized that the structural stiffness of scaffolds tested using each of the methods would also be similar. As noted above, despite the similarities in the loading and deformation conditions between the two methods, the differences which did exist led to different absolute values for loading and deformation and thus different structural stiffnesses. However, the differences in structural stiffness between two scaffold materials were similar whether the measurements were made *in vivo* or *in vitro*. It was thus demonstrated that membrane inflation testing is a simple and efficient *in vitro* testing method which can be used to measure changes in structural stiffness which are predictive of those which will exist when implanted into the right ventricle.

6.4 The Stiffness of a Biological Membrane Scaffold can be Altered Using Cell Culture Methods

The effects which alterations to three different aspects of cell culture have on scaffold stiffness were evaluated in this study. Changes in scaffold stiffness due simply to extended incubation times in cell culture media were investigated by measuring the stiffness of scaffolds after 0, 2, 4, and 10 weeks in cell culture media supplemented with 1% Penicillin/Streptomycin (P/S) and 10% Fetal Bovine Serum (FBS). The effect of cell seeding was evaluated by comparing the stiffness of scaffolds on which fibroblasts were cultured for 10 weeks with the stiffness of scaffolds incubated in cell culture media for the same period of time without any cells. Finally, the effect of media supplementation was evaluated by comparing the stiffness of scaffolds seeded with fibroblasts and incubated in media containing 50 µg/mL ascorbic acid for 10 weeks to the stiffness of scaffolds cultured with fibroblasts in standard media for the same period of time.

Extended incubation of scaffolds in cell culture media resulted in a deterioration of the scaffolds' structural properties as manifested by a decrease in modulus and an increase in thickness. Swelling has previously been shown to be a characteristic response of gelatin based scaffolds undergoing degradation (Haroun, Gamal-Eldeen, & Harding, 2009) (Dainiak, Allan, Savina, Cornelio, James, & James, 2010). Dissolution of scaffolds due to prolonged incubation in aqueous environments has also been previously reported for silk-collagen scaffolds (Lu, Wang, Lu, Li, Kaplan, & Zhu, 2010).

The culture of fibroblasts on the scaffolds resulted in a substantial increase in the modulus of the scaffolds and a decrease in their thicknesses. This was accompanied by an increase in the percentage of the scaffold mass which was comprised of collagen. Although the collagen percentage of

unaltered Veritas was not measured in this study, review of other studies revealed that the collagen percentage of pericardium-based scaffolds is in the range of 77 – 91 % as shown in Table 11.

Table 11: Comparison of collagen percentages reported in the literature to collagen percentages measured in this study

Material Preparation	Collagen (% of Dry Weight)	Reference
Acellular Bovine Pericardium	77 ± 2	(Courtman, Pereira, Kashef, McComb, Lee, & Wilson, 1994)
Acellular Human Pericardium	91.1 ± 8.5	(Mirsadraee, et al., 2006)
Veritas incubated in culture media for 10 weeks	54.1 ± 5.1	Current Study
Veritas cultured with fibroblasts for 10 weeks	83.2 ± 5.1	Current Study

It is clear from this that the presence of fibroblasts on the scaffolds results in a stabilization of the collagen percentage, in contrast to the decrease in collagen percentage which occurs when the scaffolds are incubated in culture media alone. The stabilization of the scaffolds could be due to production of new matrix, inhibition of the degradation of initial matrix, or a combination of the two. The drastic decrease in stiffness between control samples and samples cultured with fibroblasts suggests that degradation still occurs when cells are cultured on the scaffolds. Steady degradation of all matrix components would result in a decrease in the overall quantity of matrix present in the scaffold but the relative quantities of each of the matrix components would remain the same. The reduction in collagen percentage for scaffolds incubated in media therefore suggests that degradation occurs selectively for collagen. The stabilization of the collagen percentage when cells are cultured on the scaffolds may thus be due to synthesis of new collagen by the fibroblasts. Another possible mechanism by which the collagen percentage is stabilized by cells is that they inhibit scaffold degradation by producing tissue inhibitors of metalloproteinases (TIMPs) (Amalinei, Carunto, Giusca, & Balan, 2010). TIMPs inhibit the enzymes which may be present in the culture media or excreted by the cells, thus lessening the progression of degradation.

The rationale for supplementing the cell culture media with ascorbic acid was that it would induce the fibroblasts to deposit more collagen onto the scaffolds, thus enhancing the effect observed when scaffolds were cultured with fibroblasts alone. However, the addition of ascorbic acid to the media in which the fibroblast seeded scaffolds were cultured actually resulted in a decrease in the modulus of the scaffolds when compared with scaffolds cultured with fibroblasts without any ascorbic acid. This decrease in modulus was accompanied by a decrease in the amount of acid/pepsin soluble collagen. Scaffolds cultured with fibroblasts in media supplemented with ascorbic acid appeared to exhibit the same trends as scaffolds cultured with fibroblasts in standard media but to a lesser magnitude. There was a decrease in thickness and an increase in total collagen over that measured for unseeded scaffolds but the magnitudes of both of these changes were less than that measured for scaffolds cultured with fibroblasts in standard media. The increase in total collagen was correlated with an increase in elastic modulus, which again was greater than that measured for unseeded scaffolds but less than that

measured for scaffolds seeded with fibroblasts in standard media. The exception to this pattern was for the observed trend in which fibroblast-seeded scaffolds had a lower ratio of acid/pepsin soluble collagen to total collagen and a lower area stretch ratio at failure. Instead of following this same trend, but to a lesser degree, the scaffolds cultured with fibroblasts in ascorbic acid supplemented media had the lowest ratio of acid/pepsin soluble collagen to total collagen and the lowest area stretch ratio at failure. It appears that the ratio of acid/pepsin soluble collagen to total collagen plays an important role in the degree to which scaffolds deform at failure. Scaffolds for which less of the collagen was enzymatically degradable had lower deformations at failure. It is possible that this is a result of increased collagen cross-linking due to the presence of ascorbic acid.

Despite the initial strength and structural stability of the pericardium-based scaffold (Veritas) used in this study, it was demonstrated that exposure to a variety of cell culture conditions could have a drastic impact on the mechanical properties of the material. It should be noted that Veritas and other tissue-derived scaffolds undergo substantial manipulation during production in order to decellularize, sterilize, and ensure biocompatibility of the scaffolds. Each of these steps alters the material in some way and results in changes to the mechanical properties of the material (Rosario D. , Reilly, Salah, Glover, Bullock, & MacNeil, 2008). Thus, an alternate method to that proposed in this study for changing the mechanical properties of a scaffold is to tailor the production process to achieve the desired mechanical properties. For example, decellularization is often achieved by incubating the material in a salt or acid solution. Collagen is soluble in these solutions and some degree of scaffold degradation thus occurs in these steps. Extending the incubation time in these solutions or increasing their strength would result in more pronounced degradation and thus a further reduction in the mechanical properties of the materials. Enzymatic treatments are also used in the production of many natural biomaterial scaffolds and application of an enzymatic treatment to a biological membrane scaffold such as Veritas would result in reduction of the scaffold stiffness. These methods would likely have similar results to those found in this study for the scaffolds cultured in media alone, but in a much shorter amount of time. Enzymatic manipulations operate by removing material from the scaffolds, potentially resulting in a change in biochemical composition as some components are enzymatically degraded while others are not. In contrast, the method proposed in this study by which cells are cultured on the scaffolds maintains biochemical composition while still achieving a change in stiffness, due likely to an overall reduction of material and alteration of matrix structure.

6.4.1 Is the Strength of Tissue Engineered Scaffolds Sufficient?

The tissue engineered scaffolds developed in this project had stiffness values in the same range as that of cardiac tissue. However, the same cellular processes which lower the stiffness values of the tissue engineered scaffolds into a physiological range also reduce the failure tension of the samples. Figure 44 shows a comparison of the failure tensions of the tissue engineered scaffolds to the tension which occurs in the canine right ventricle at end-systole. The tension in the canine right ventricle at end-systole was determined by multiplying the average maximum pressure (17.2 ± 1.8) by the average radius of curvature (56.6 ± 5.6 mm).

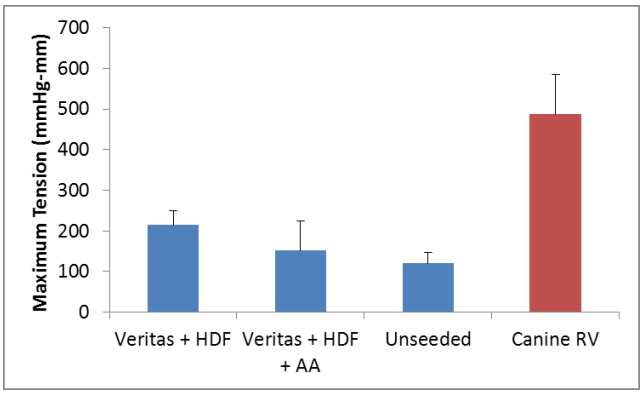

Figure 44: Tissue engineered scaffolds burst at tensions is which were lower than the maximum tension which occurs in the canine right ventricle

It is clear from this that the scaffolds would not be suitable for implantation into a large animal such as a canine. It is interesting to note that stiffness is more sensitive to tissue engineering manipulation than failure tension. There is a seven-fold difference in mean stiffness of the Veritas + HDF group and the unseeded group while there is less than a two-fold difference in failure tension. Thus the presence of fibroblasts is able to inhibit a decrease in stiffness due to degradation but is unable to add substantial structural integrity.

Chapter 7: Future Work and Implications

The scaffolds tested in this study were carried out to ten weeks because pilot studies showed no detectable differences between seeded and unseeded scaffolds at earlier time points. The result of carrying the experiment out to time points at which differences in stiffness could be detected was that the failure properties of the scaffolds also deteriorated to impractically low levels. In addition, the long incubation period used in this study is impracticle from a commercialization perspective due to the materials and labor involved. This could be addressed in the future by examining the time points between four and ten weeks to determine how long the scaffolds can be exposed to culture conditions before their failure properties become unacceptable. This time point should be used as a starting point to begin altering the stiffness of the scaffolds by cell seeding. One likely reason that an effect of cell seeding on stiffness was not observed at early time points is that the bulk of the scaffold is still intact due to little degradation occurring. With this bulk of the sample intact the number and types of cells used in this experiment were unable to have a detectable impact on the stiffness of the scaffolds. This could be addressed by seeding the scaffolds with a greater number of cells, seeding them with cell types which produce more extracellular matrix, or supplementing the culture medium with growth factors to induce greater production of extracellular matrix by the cells.

Ideally, the stiffness of heart tissue would have been measured *in vivo* and used as a control value to which the stiffness values of tissue engineered scaffolds could be compared. Unfortunately, this data was not available and it was thus necessary to convert to elastic modulus and compare to literature values. Further work should be done to obtain HDM and pressure data of control heart tissue and analyze the data according to the methods used in this project.

This approach to scaffold fabrication is ideal in that the scaffolds could be decellularized and sterilized after manipulation is complete. One challenge which may need to be addressed is the variability between cell seeded scaffolds which could occur due to differences in cell metabolism. However, the sample to sample variation which exists currently due to differences in physiology and anatomy between animals is likely to be a more substantial contributor to overall variability.

Conclusions

The goals of this study were to demonstrate that the stiffness of biological cardiac scaffolds can be measured *in vitro* and that it can be altered using cell culture techniques. It was first demonstrated that membrane inflation testing is a suitable method for testing the stiffness of cardiac scaffolds which yields differences between materials which are similar to those obtained when testing the scaffold *in vivo*. It was then found that the stiffness of a biological scaffold decreases over time when incubated in cell culture media without any cells. When cells were cultured on the biological scaffold the decrease in stiffness was not as large. Thus, the stiffness of biological scaffolds can be decreased through exposure to cell culture media and then increased by culturing with cells. The biochemical behavior which caused the changes in stiffness was also investigated. It was found that cell seeded scaffolds were more compacted, had a greater percentage of total collagen, and that less of the collagen was susceptible to enzymatic degradation. In addition to its impact on stiffness, the low amount of enzymatically degradable collagen in the cell seeded scaffolds caused them to be less extensible than unseeded scaffolds.

References

Adhyapak, S. M., & Parachuri, V. R. (2010). Architecture of the left ventricle: insights for optimal surgical ventricular restoration. *Heart Fail Rev, 15*, 73-83.

Aetna. (2009, April 3). Clinical Policy Bulletins: Ventricular Remodeling Operation (Batista Procedure)/and Surgical Ventricular Restoration (Dor Procedure) (Policy #0182).

Ahlfors, J.-E. W., & Billiar, K. L. (2007). Biomechanical and biochemical characteristics of a human fibroblast-produced and remodeled matrix. *Biomaterials, 28*, 2183-2191.

Amalinei, C., Carunto, I.-D., Giusca, S. E., & Balan, R. A. (2010). Matrix Metalloproteinases Involvement in Pathologic Conditions. *Romanian Journal of Morphology and Embryology, 51*(2), 215-228.

American Heart Association. (2008). *Heart Disease and Stroke Statistics.* American Heart Association, Dallas, Texas.

Androjna, C., Spragg, R. K., & Derwin, K. A. (2007). Mechanical Conditioning of Cell-Seeded Small Intestine Submucosa: A Potential Tissue-Engineering Strategy for Tendon Repair. *Tissue Engineering, 13*(2), 233-243.

Athanasuleas, C. L., Buckberg, G. D., Stanley, A. W., Siler, W., Dor, V., & Di Donato, M. (2004). Surgical Ventricular Restoration in the Treatment of Congestive Heart Failure Due to Post-Infarction Ventricular Dilation. *Journal of the American College of Cardiology, 44*(7), 1439-1445.

Azeloglu, E. U., Yun, Y. H., Saltman, A. E., Krukenkamp, I. B., Chiang, F., & Chen, W. (2006). High resolution mechanical function in the intact porcine heart: mechanical effects of pacemaker location. *Journal of Biomechanics, 39*, 717-725.

Badylak, S. F., Kochupura, P. V., Cohen, I. S., Doronin, S. V., Saltman, A. E., & Gilbert, T. (2006). The Use of Extracellular Matrix as an Inductive Scaffold for the Partial Replacement of Functional Myocardium. *Cell Transplantation, 15 Supplement 1*, 100-112.

Balestrini, J. L., & Billiar, K. L. (2006). Equibiaxial cyclic stretch stimulates fibroblasts to rapidly remodel fibrin. *Journal of Biomechanics, 39*, 2983-2990.

Batista, R. J., Verde, J., Nery, P., Bocchino, L., Takeshita, N., Bhayana, J. N., et al. (1997). Partial Left Ventriculectomy to Treat End-Stage Heart Disease. *Ann Thorac Surg, 64*, 634-638.

Bax, J. J., Schinkel, A. F., Boersma, E., Elhendy, A., Vittoria, R., Maat, A., et al. (2004). Extensive Left Ventricular Remodeling Does Not Allow Viable Myocardium to Improve in Left Ventricular Ejection Fraction After Revascularization and Is Associated With Worse Long-Term Prognosis. *Circulation, 110*, II18-II22.

Billiar, K. L., Throm, A., & Frey, M. T. (2005). Biaxial failure properties of planar living tissue equivalents. *J Biomed Mater Res, 73A*, 182-191.

Buckberg, G. D. (2007). Ventricular structures must be understood during surgical restoration for heart failure. *Scandinavian Journal of Surgery, 96*, 164-176.

Buckberg, G. D., & Athanasuleas, C. L. (2009, November). The STICH trial: Misguided conclusions. *The Journal of Thoracic and Cardiovascular Surgery*, 1060-1064.

Buckberg, G. D., & Group, t. R. (2006). Form versus disease: optimizing geometry during ventricular restoration. *European Journal of Cardio-thoracic Surgery, 29S*, S238-S244.

Buckberg, G. D., & Group, t. R. (2006). The ventricular septum: the lion of right ventricular function, and its impact on right ventricular restoration. *Eur J Cardiothorac Surg, S29*, S272-S278.

Chan, D., Lamande, S. R., Cole, W. G., & Bateman, J. F. (1990). Regulation of procollagen synthesis and processing during ascorbate-induced extracellular matrix accumulation in vitro. *Biochem. J., 269*, 1750181.

Cigna. (2010, March 15). Cigna Medical Coverage Policy: Partial Left Ventriculectomy, Dynamic Cardiomyoplasty and Ventricular Reshaping in the Treatment of Heart Failure (Policy #0312).

Cooley, D., Collins, H., Morris, G., & Chapman, D. (1958). Ventricular aneurysm after myocardial infarction; surgical excision with use of temporary cardiopulmonary bypass. *Journal of the American Medical Association, 167*(5), 557-560.

Coskun, K. O., Popov, A. F., Coskun, S. T., Hinz, J., Schmitto, J. D., & Körfer, R. (2009). Surgical Treatment of Left Ventricular Aneurysm. *Asian Cardiovasc Thorac Ann, 17*, 490-493.

Courtman, D., Pereira, C., Kashef, V., McComb, D., Lee, J., & Wilson, G. (1994). Development of a pericardial acellular matrix biomaterial: Biochemical anc mechanical effects of cell extraction. *Journal of Biomedical Materials Research, 28*, 655-666.

Cox, J. I. (2004). Cardiac Surgery for Arrhythmias. *J Cardiovasc Electrophysiol, 15*, 250-262.

Dahms, S. E., Piechota, H., Dahiya, R., Lue, T., & Tanagho, E. (1998). Composition and biomechanical properties of the bladder acellular matrix graft: comparative analysis in rat, pig and human. *British Journal of Urology, 82*, 411-419.

Dainiak, M. B., Allan, I. U., Savina, I. N., Cornelio, L., James, E. S., & James, S. L. (2010). Gelatin-fibrinogen cryogel dermal matrices for wound repair: Preparation, optimization, and in vitro study. *Biomaterials, 31*, 67-76.

Di Donato, M., Castelvecchio, S., & Menicanti, L. (2010). End-systolic volume following surgical ventricular reconstruction impacts survival in patients with ischaemic dilated cardiomyopathy. *European Journal of Heart Failure, 12*, 375-381.

Di Donato, M., Sabatier, M., Dor, V., Gensini, G. F., Toso, A., Maioli, M., et al. (2001). Effects of the Dor Procedure on Left Ventricular Dimension and Shape and Geometric Correlates of Mitral

Regurgitation One Year After Surgery. *The Journal of Thoracic and Cardiovascular Surgery, 121*, 91-96.

Di Donato, M., Toso, A. D., Sabatier, M., Barletta, G., Menicanti, L., Fantini, F., et al. (2004). Surgical Ventricular Restoration Improves Mechanical Intraventricular Dyssynchrony in Ischemic Cardiomyopathy. *Circulation, 109*, 2536-2543.

Discher, D. E., Janmey, P., & Wang, Y.-l. (2005). Tissue Cells Feel and Respond to the Stiffness of Their Substrate. *Science, 310*, 1139-1143.

Dor, V., Sabatier, M., & Montiglio, F. (2004). Endoventricular Patch Reconstruction of Ischemic Failing Ventricle. A Single Center with 20 years Experience. Advantages of Magnetic Resonance Imaging Assessment. *Heart Failure Reviews, 9*, 269-286.

Editorial Comment. (2010). Surgical planning for surgical ventricular restoration involves decision options on form versus disease. *European Journal of Cardio-thoracic Surgery, In Print*.

Elsheikh, A., & Anderson, K. (2005). Comparative study of corneal strip extensometry and inflation tests. *J. R. Soc. Interface, 2*, 177-185.

Engler, A. J., Sen, S., Sweeney, H. L., & Discher, D. E. (2006, August 25). Matrix Elasticity Directs Stem Lineage Specification. *Cell, 126*, 677-689.

European Society of Cardiology. (2008). ESC Guidelines for the diagnosis and treatment of acute and chronic heart failure 2008. *European Heart Journal, 29*, 2388-2442.

Feneley, M. P., Elbeery, J. R., Gaynor, J. W., & Gall Jr., S. A. (1990). Ellipsoidal Shell Subtraction Model of Right Ventricular Volume. *Circulation Research, 67*, 1427-1436.

Filipe, D. V., McBride, N. S., Murphy, M. K., & Singh, D. A. (2007). *Design of a Composite Scaffold for Myocardial Regeneration.* Worcester Polytechnic Institute, Biomedical Engineering. Worcester: Worcester Polytechnic Institute.

Freytes, D. O., Rundellc, A. E., Vande Geest, J., & Vorp, D. A. (2005). Analytically derived material properties of multilaminated extracellular matrix devices using the ball-burst test. *Biomaterials, 26*, 5518–5531.

Freytes, D. O., Tullius, R. S., & Badylak, S. F. (2006). Effect of Storage Upon Material Properties of Lyophilized Porcine Extracellular Matrix Derived From the Urinary Bladder. *J Biomed Mater Res Part B: Appl Biomater, 78B*, 327-333.

Gaudette, G. R., & Cohen, I. S. (2006). Cardiac Regeneration: Materials Can Improve the Passive Properties of Myocardium, but Cell Therapy Must Do More. *Circulation, 114*, 2575-2577.

Gaudette, G. R., Todardo, J., Krukenkamp, I. B., & Chiang, F.-P. (2001). Computer Aided Speckle Interferometry: A Technique for Measuring Deformation of the Surface of the Heart. *Annals of Biomedical Engineering, 29*, 775-780.

Gentleman, E., Lay, A. N., Dickerson, D. A., & Nauman, E. A. (2003). Mechanical characterization of collagen fibers and scaffolds for tissue engineering. *Biomaterials, 24*, 3805-3813.

Gilbert, T. W., Stewart-Akers, A. M., Sydeski, J., Nguyen, T. D., Badylak, S. F., & Woo, S. L.-Y. (2007). Gene Expression by Fibroblasts Seeded on Small Intestinal Submucosa and Subjected to Cyclic Stretching. *Tissue Engineering, 13*(6), 1-11.

Gilbert, T. W., Wognum, S., Joyce, E. M., Freytes, D. O., & Sacks, M. S. (2008). Collagen fiber alignment and biaxial mechanical behavior of porcine urinary bladder derived extracellular matrix. *Biomaterials, 29*, 4775–4782.

Haroun, A. A., Gamal-Eldeen, A., & Harding, D. R. (2009). Preparation, characterization, and in vitro biological study of biomimetic three-dimensional gelatin-montmorillonite/cellulose scaffold for tissue engineering. *J Mater Sci: Mater Med, 20*, 2527-2540.

Heerebeek, L. v., Hamdani, N., Handoko, M. L., Falcao-Pires, I., Musters, R. J., & Kupreishvili, K. (2008). Diastolic Stiffness of the Failing Diabetic Heart: Importance of Fibrosis, Advanced Glycation End Products,and Myocyte Resting Tension. *Circulation, 117*, 43-51.

Ignat'eva, N. Y., Danilov, N. A., Averkiev, S. V., Obrezkova, M. V., Lunin, V. V., & Sobol, E. N. (2007). Determination of Hydroxyproline in Tissues and the Evaluation of the Collagen Content of the Tissues. *Journal of Analytical Chemistry, 62*(1), 51-57.

Ishikawa, O., Kondo, A., Okada, K., Miyachi, Y., & Furmira, M. (1997). Morphological and biochemical analyses on fibroblasts and self-produced collagens in a novel three-dimensional culture. *British Journal of Dermatology, 136*, 6-11.

Jaber, W. A., Lam, C. S., Meyer, D. M., & Redfield, M. M. (2007). Revisiting methods for assessing and comparing left ventricular diastolic stiffness: impact of relaxation, external forces, hypertrophy, and comparators. *Am J Physiol Heart Circ Physiol, 293*, H2738–H2746.

Jones, R. H., Eric J. Velazquez, M. M., Sopko, G., Oh, J. K., & O'Connor, C. M. (2009, April 23). Coronary Bypass Surgery with or without Surgical Ventricular Reconstruction. *The New England Journal of Medicine, 360*(17), 1705-1717.

Kalkat, M. S., Dandekar, U., Smallpeice, C., Parmar, J., Satur, C., & Levine, A. (2006). Left Ventricular Aneurysmectomy: Tailored Scar Excision and Linear Closure. *Asian Cardiovasc Thorac Ann, 14*, 231-234.

Kaza, A. K., Patel, M. R., Fiser, S. M., Long, S. M., Kern, J. A., Tribble, C. G., et al. (2002). Ventricular Reconstruction Results in Improved Left Ventricular Function and Amelioration of Mitral Insufficiency. *Annals of Surgery, 6*, 828-832.

Kelly, D. J., Rosen, A. B., Schuldt, A. J., Kochupura, P. V., Doronin, S. V., & Potapova, I. A. (2009). Increased Myocyte Content and Mechanical Function Within a Tissue-Engineered Myocardial Patch Following Implantation. *Tissue Engineering Part A, 15*(8), 2189-2201.

Kieser, T. M. (2009, September). Letter to the Editor: The Left Ventricle: To Reconstruct or Not - Lessons from the STICH Trial. *The Journal of Thoracic and Cardiovascular Surgery*, 784.

Kim, B.-S., Nikolovski, J., Bonadio, J., & Mooney, D. J. (1999, October). Cyclic mechanical strain regulates the development of engineered smooth muscle tissue. *Nature Biotechnology, 17*, 979-983.

Kochupura, P. V., Azeloglu, E. U., Kelly, D. J., Doronin, S. V., Badylak, S. F., Krukenkamp, I. B., et al. (2005). Tissue-Engineered Myocardial Patch Derived From Extracellular Matrix Provides Regional Mechanical Function. *Circulation, 112 Suppl I*, I144-I149.

Lillehei, C. W., Levy, M. J., Dewall, R. A., & Warden, H. E. (1962). Resection of Myocardial Aneurysms after Infarction during Temporary Cariopulmonary Bypass. *Cirulation, 26*, 206-217.

Lim, K. O., & Boughner, D. (1976). The Low Frequency Dynamic Viscoelastic Properties of Human Aortic Valve Tissue. *Circulation Research*, 209-214.

Long, R. A., Nagatomia, J., Chancellor, M. B., & Sacks, M. S. (2006). The role of MMP-I up-regulation in the increased compliance in muscle-derived stem cell-seeded small intestinal submucosa. *Biomaterials, 27*, 2398-2404.

Lu, Q., Wang, X., Lu, S., Li, M., Kaplan, D. L., & Zhu, H. (2010). Nanofibrous architecture of silk fibroin scaffolds prepared with a mild self-assembly process. *Biomaterials, Article in Press*, 1-9.

Lu, S.-H., Sacks, M. S., Chung, S. Y., Gloeckner, D. C., Pruchnic, R., Huard, J., et al. (2005). Biaxial mechanical properties of muscle-derived cell seeded small intestinal submucosa for bladder wall reconstitution. *Biomaterials, 26*, 443-449.

Lundblad, R., Abdelnoor, M., & Svennevig, J. L. (2004). Surgery for left ventricular aneurysm: Early and late survival after simple linear repair and endoventricular patch plasty. *Surgery for Acquired Cardiovascular Disease, 128*, 449-456.

Mark, D. B., Knight, J. D., Velazquez, E. J., Howlett, J. G., Spertus, J. A., & Djokovic, L. T. (2009). Quality of life and economic outcomes with surgical ventricular reconstruction in ischemic heart failure: Results from the Surgical Treatment for Ischemic Heart Failure trial. *American Heart Journal, 157*, 837-844.

Marra, S. P., Kennedy, F. E., Kinkaid, J. N., & Fillinger, M. F. (2006). Elastic and Rupture Properties of Porcine Aortic Tissue Measured Using Inflation Testing. *Cardiovasc Eng, 6*, 125-133.

McCarthy, J. F., McCarthy, P. M., Starling, R. C., Smedira, N. G., Scalia, G. M., & Wong, J. (1998). Partial left ventriculectomy and mitral valve repair for end-stage congestive heart failure. *European Journal of Cardio-thoracic Surgery, 13*, 337-343.

Mirsadraee, S., Wilcox, H., Korossis, S., Kearney, J., Watterson, K., Fisher, J., et al. (2006). Development and Characterization of an Acellular Human Pericardial Matrix for Tissue Engineering. *Tissue Engineering, 12*(4), 763-773.

Moulton, M. J., Creswell, L. L., Actis, R. L., Myers, K. W., Vannier, M. W., & Szabo, B. A. (1995). An inverse approach to determining myocardial material properties. *Journal of Biomechanics, 28*(8), 935-948.

Nagueh, S. F., Shah, G., Wu, Y., Torre-Amione, G., King, N. M., & Lahmers, S. (2004). Altered Titin Expression, Myocardial Stiffness, and Left Ventricular Function in Patients With Dilated Cardiomyopathy. *Circulation, 110*, 155-162.

Pasipoularides, A., Shu, M., Shah, A., Silvestry, S., & Glower, D. D. (2002). Right ventricular diastolic function in canine models of pressure overload, volume overload, and ischemia. *Am J Physiol Heart Circ Physiol, 283*, H2140-H2150.

Pearson, R., Philips, N., Hancock, R., Hashim, S., Field, M., & Richens, D. (2008). Regional wall mechanics and blunt traumatic aortic rupture at the isthmus. *European Journal of Cardio-thoracic Surgery, 34*, 616-622.

Pocar, M., Di mauro, A., Passolunghi, D., Moneta, A., Alsheraei, A. M., & Bregasi, A. (2010). Predictors of adverse events after surgical ventricular restoration for advanced ischaemic cardiomyopathy. *European Journal of Cardio-thoracic Surgery, In Print*.

Robinson, K. A., Li, J., Mathison, M., Redkar, A., Cui, J., & Chronos, N. A. (2005). Extracellular Matrix Scaffold for Cardiac Repair. *Circulation, 112*, 135-143.

Rosario, D. J., Reilly, G. C., Salah, E. A., Glover, M., Bullock, A. J., & MacNeil, S. (2008). Decellularization and sterilization of porcine urinary bladder matrix for tissue engineering in the lower urinary tract. *Regen Med, 3*(2), 145-156.

Rosario, D., Reilly, G., Salah, E., Glover, M., Bullock, A., & MacNeil, S. (2008). Decellularization and sterilization of porcine uriinary bladder matrix for tissue engineering in the lower urinary tract. *Regenerative Medicine, 3*(2), 145-156.

Sallin, E. A. (1969). Fiber Orientation and Ejection Fraction in the Human Left Ventricle. *Biophysical Journal, 9*, 954-964.

Slifka, A., Drexler, E., Wright, J., & Shandas, R. (2006). Bubble-test method for synthetic and bovine vascular material. *Journal of Biomechanics, 39*, 1939-1942.

Smits, L., Ozolanta, I., Ozolins, V., Lacis, A., & Kasyanov, V. (2008). Biomechanical Properties of Two Synthetic Biomaterials for Ventricular Septal Defect Closure in Infants. *IFMBE Proceedings, 20*, 76-79.

Suma, H., Horii, T., Isomura, T., Buckberg, G., & Group, t. R. (2006). A new concept of ventricular restoration for nonischemic dilated cardiomyopathy. *Eur J Cardiothorac Surg, 29*, 207-212.

Throm, A. M., Liu, W.-C., Lock, C.-H., & Billiar, K. L. (2010). Development of a cell-derived matrix: Effects of epidermal growth factor in chemically defined culture. *J Biomed Mater Res, 92A*, 533-541.

Tønnessen, T., & Knudsen, C. W. (2005). Surgical left ventricular remodeling in heart failure. *The European Journal of Heart Failure, 7*, 704-709.

Tullberg-Reinert, H., & Jundt, G. (1999). In situ measurement of collagen synthesis by human bone cells with a Sirius Red-based colorimetric microassay: effects of transforming growth factor b2 and ascorbic acid 2-phosphate. *Histochem Cell Biol, 112*, 271–276.

Ueno, T., Sakata, R., Iguro, Y., Yamamoto, H., Ueno, M., & Ueno, T. (2007). Mid-term changes of left ventricular geometry and function after Dor, SAVE, and Overlapping procedures. *European Journal of Cardio-thoracic Surgery, 32*, 52-57.

Wall, S. T., Walker, J. C., Healy, K. E., Ratcliffe, M. B., & Guccione, J. M. (2006). Theoretical Impact of the Injection of Material Into the Myocardium: A Finite Element Model Simulation. *Circulation, 114*, 2627-2635.

White, H. D., Norris, R. M., Brown, M. A., Brandt, P. W., Whitlock, R. M., & Wild, C. J. (1987). Left ventricular end-systolic volume as the major determinant of survival after recovery from myocardial infarction. *Circulation, 76*, 44-51.

Xue, L., & Greisler, H. P. (2003). Biomaterials in the development and future of vascular grafts. *Journal of Vascular Surgery, 37*(2), 472-480.

Yamamoto, I., Muto, N., Murakami, K., & Akiyama, J.-I. (1992). Collagen Synthesis in Human Skin Fibroblasts is Stimulated by a Stable Form of Ascorbate, 2-O-a-D-Glucopyranosyl-L-Ascorbic Acid. *J Nutr, 122*, 871-877.

Zeltsman, D., & Acker, M. A. (n.d.). Surgical Management of Heart Failure: An Overview. *Annu. Rev. Med., 53*, 383-391.

Zoffoli, G., Manino, D., Venturini, A., Terrini, A., Asta, A., & Zanchettin, C. (2009). Diagnosing left ventricular aneurysm from pseudo-aneurysm: a case report and a review in literature. *Journal of Cardiothoracic Surgery, 4*(11).

Appendix A: Determination of Ascorbic Acid Concentration

Methods

Adult human dermal fibroblasts were plated at a density of 10,000 cells/well in 24 well plates. After 24 hours in DMEM supplemented with 10% FBS and 1% P/S, fresh media was added containing 0, 50, or 300 µg/mL of ascorbic acid. Media was replaced every 4-5 days.

Cell viability, cell number, collagen in culture medium, and collagen in the cell layer were measured after 2 and 14 days of incubation. At each time point 100µL of culture medium was removed from each well and retained for analysis of soluble collagen by the Sircol assay. The remaining media was aspirated and the samples were incubated in a solution of Alamar Blue dye to assess the metabolic activity of the cells. During a 2 hour incubation period the dye was reduced from its initial blue color to a bright pink color and samples were taken for absorbance measurements. The remaining media was aspirated and a Hoescht dye solution was added to each well to estimate cell number through quantification of total DNA. The media in each well was aspirated and plates were processed for analysis of collagen in the cell layer using the Sirius Red assay

The Sircol assay was used to quantify the amount of soluble collagen in 100µL samples of culture media. To avoid interference due to the high FBS concentration, collagen was precipitated by adding 900µL of 4.4M NaCl to each 100µL sample and centrifuging at 14,000rpm for 10 minutes. The supernatant was discarded and the pellet containing purified collagen was resuspended in 0.5M acetic acid. One milliliter of Sirius Red dye reagent (1mg/mL Direct Red 80 Dye in Picric Acid) was added to each sample and incubated under gentle agitation for 30 minutes at room temperature. The supernatant containing unbound dye was discarded and the pellet comprised of the collagen-dye complex was solubilized with 1mL of 0.5N NaOH. One-hundred microliter aliquots of each sample were transferred in triplicate to a 96 well plate and the absorbance at 550nm was recorded. A standard curve of collagen (1mg/mL in 5mM HCl) derived from rat tail tendon was used to relate absorbance to collagen concentration.

The Alamar Blue assay measures the ability of cells to reduce the Alamar Blue dye and can thus be used to assess their metabolic activity. The media in each well was replaced with a 1:10 solution of Alamar Blue dye in serum free DMEM and incubated at 37°C for 2 hours. One-hundred microliter aliquots of each sample were transferred in triplicate to a 96 well plate and the absorbance at 570nm and 600nm was recorded. A standard curve was prepared by plating cells of the same passage as used for experimental samples in a 24 well plate at concentrations ranging from 0-150,000 cells/mL. The assay was run on the standard curve after culturing the cells for 24 hours in DMEM supplemented with 10% FBS and 1% P/S.

The Hoescht dye binds to the DNA of cells and can thus be used to estimate cell number. Four-hundred microliters of a 1:6000 solution of Hoescht dye in 1X Phosphate Buffered Saline (PBS) was added to each well. After a 30 minute incubation at 37°C the fluorescence of each well was measured using a fluorescence plate reader.

The Sirius Red assay was used to measure the amount of collagen deposited by cells in their extracellular matrix. Samples were prepared by washing three times with 1X PBS and fixing for 1 hour in Bouin's solution. This solution was aspirated and the plates were placed under running water for 15 minutes to ensure that all of the solution was removed. The plates were placed in a vacuum chamber until fully dry and transferred to a desiccator for storage. One-hundred microliters of Sirius Red dye solution (1mg/mL Direct Red 80 dye in Picric Acid) was added to each well and incubated under gentle agitation at room temperature for 1 hour. Each well was washed three times with 0.01N HCl to remove any unbound dye before adding 100µl of 0.1N NaOh to dissolve the dye bound to the cell layer. The absorbance of these wells at 550nm was then measured. To relate these absorbencies to collagen concentration a standard curve of collagen derived from rat tail tendon and diluted to concentrations of 0-10µg/ml in 5mM HCl was used. One hundred microliters of the collagen solutions were placed in triplicate in a 96-well plate and dried onto the surface of the well by placing in a desiccator overnight. The standard curve was analyzed according to the same protocol as described above and the linear relationship between absorbance and collagen concentration was established. Phase contrast light microscopy was also used to visualize the amount of collagen present in the cell layer.

Based on the outcome of this study a concentration of 50 µg/mL was used in further studies.

Results

An optimal ascorbic acid concentration was identified by measuring cell viability, cell number, collagen present in culture media, and collagen present in the cell layer. The plots in Figure 45 show the effects of ascorbic acid on cell viability and cell number after 2 and 14 days in culture.

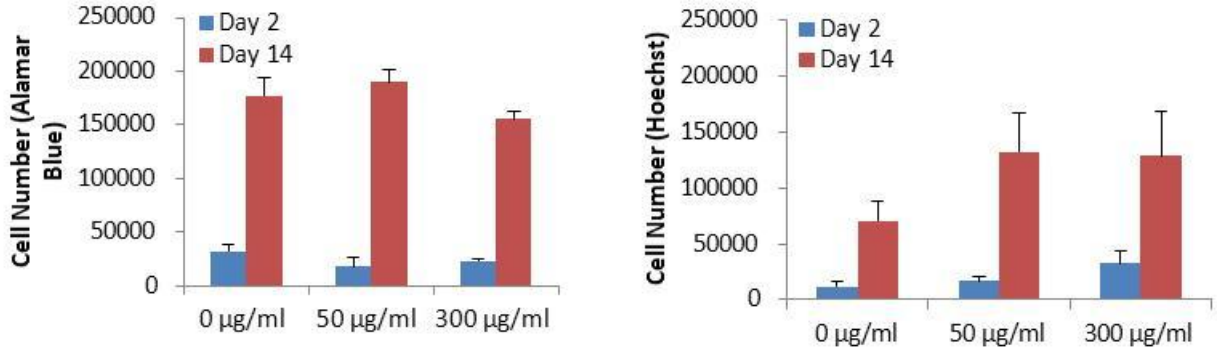

Figure 45: Cell viability (left) and cell number (right)

The concentrations of ascorbic acid tested do not have a significant effect on the amount of collagen in the culture medium as shown in Figure 46 in the plot on the left. The amount of collagen incorporated into the cell layer does vary however as shown in Figure 46 in the plot on the right.

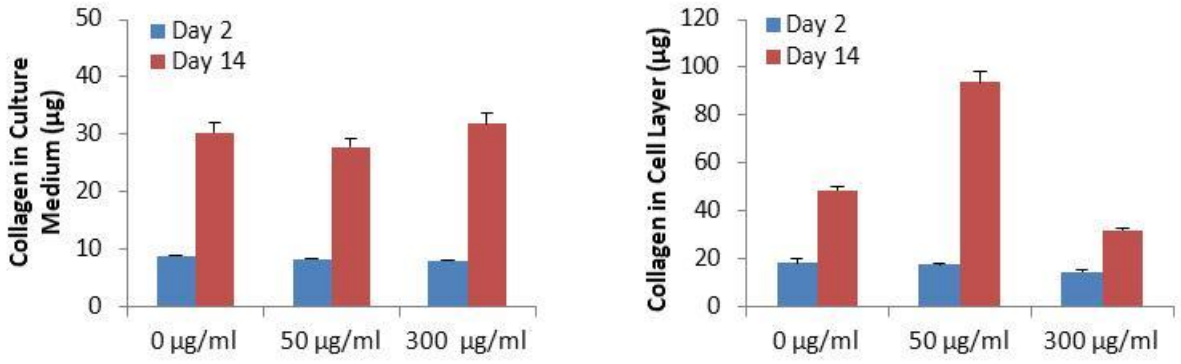

Figure 46: Collagen in culture medium (left) and in cell layer (right)

These results are confirmed by images taken of the stained cell layers as shown in Figure 47 where the amount of red staining corresponds to the amount of collagen in the cell layer.

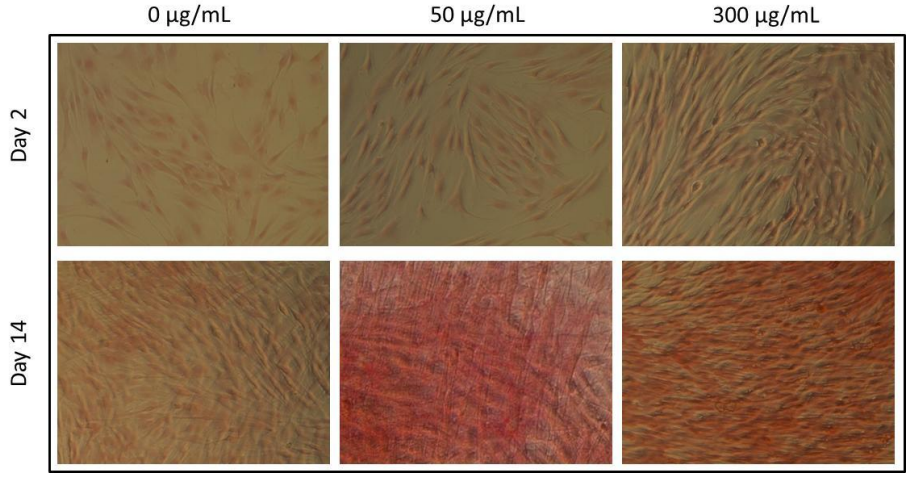

Figure 47: Fibroblasts treated with varying concentrations of ascorbic acid for 2 or 14 days (20X)

An ascorbic acid concentration of 50µg/mL appears to significantly increase the amount of collagen in the cell layer. Concentrations above this do not appear to appreciably increase the amount of collagen present.

Appendix B: Correlations between Collagen and Mechanical Properties

The correlation coefficients between each of the mechanical properties and total collagen, acid/pepsin soluble collagen, and the ratio between the two are shown in the figure below.

	Correlation Coefficient		
Parameter	**Total Collagen**	**Acid/Pepsin Soluble Collagen**	**Ratio**
Thickness	-0.76	-0.22	0.34
Stiffness	0.34	0.25	-0.09
Stress at Failure	0.62	0.32	-0.10
Tension at Failure	0.29	0.16	-0.12
Area Stretch Ratio at Failure	-0.73	0.50	0.79
Radius of Curvature at Failure	0.49	-0.59	-0.69

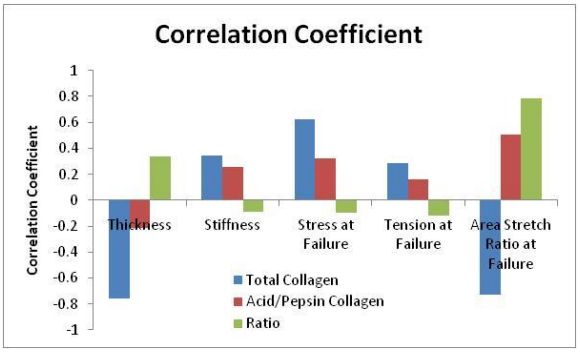

Plots of the parameters with weak correlations are shown in the following figures. The correlations of stiffness, stress at failure, and tension at failure with total collagen appear to be weak primarily due to the presence of outliers.

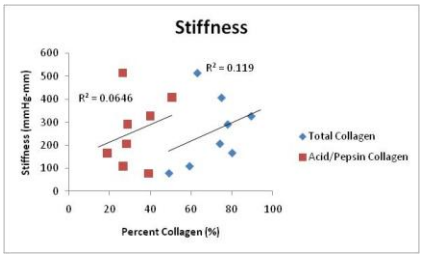

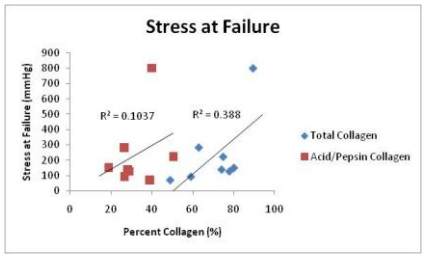

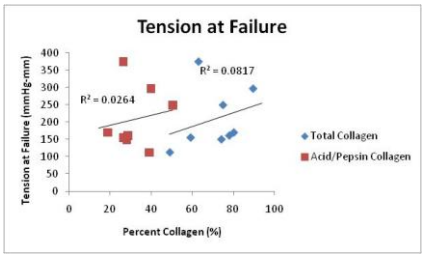

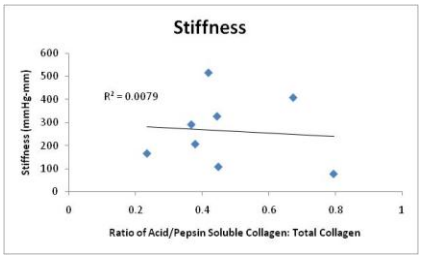

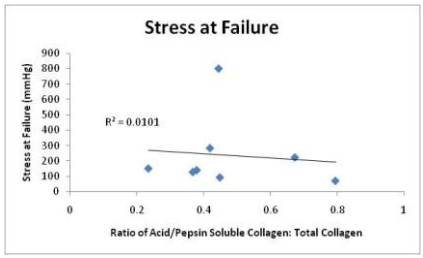

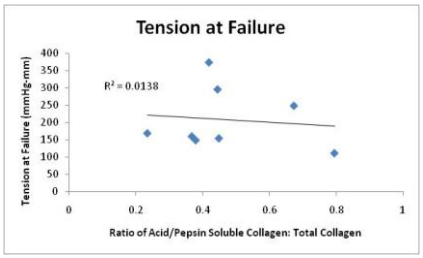

Appendix C: Alamar Blue Staining

Images of representative samples are shown in the figure below.

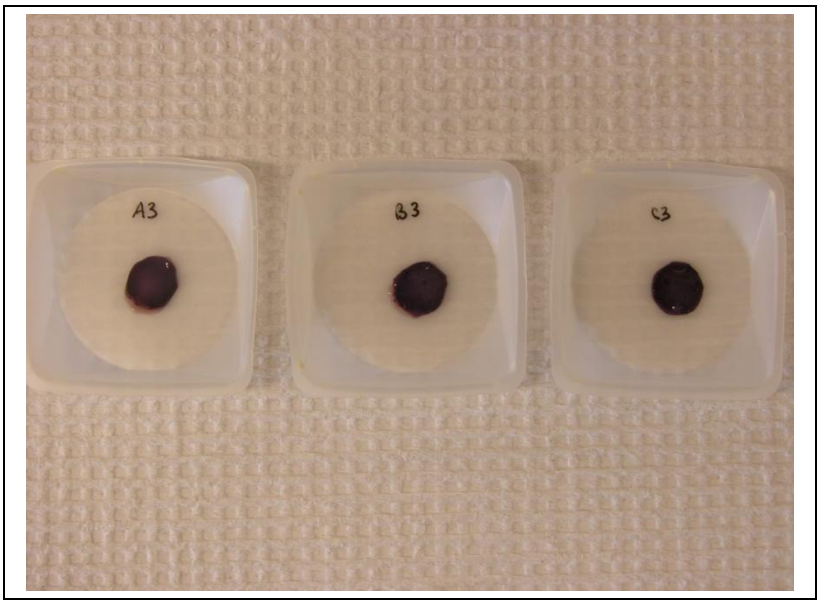

The dark stained regions suggest that viable cells remain on the scaffolds after the culture time of 10 weeks.

Appendix D: Pilot Study: Cell Seeding of Veritas

Fibroblasts grown on Veritas for 2 weeks at an initial seeding density of 2,500 cells/mm^2 were stained with calcein dye (live stain from live/dead assay). Results demonstrated that the cells remain viable and were well incorporated into the scaffold, suggesting that they may be responsible for the observed changes in mechanical properties. A representative image is shown below.

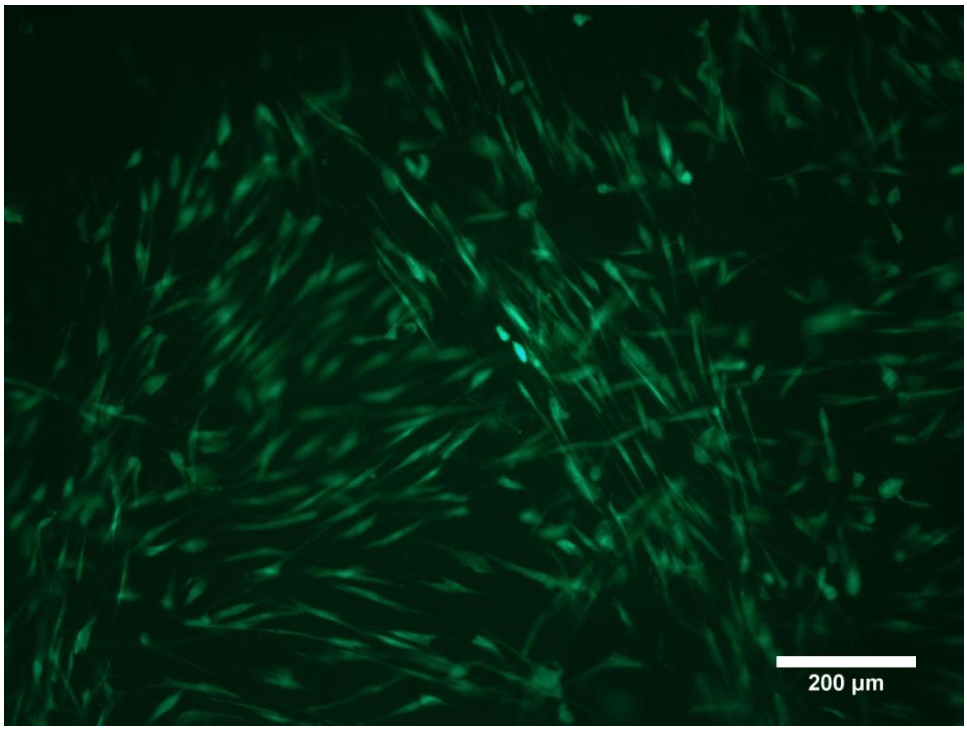

Mechanical properties of the scaffolds are shown in the plots below. A longer incubation times was chosen since the stiffness's of unseeded and seeded scaffolds at 2 and 4 weeks were too close to distinguish.

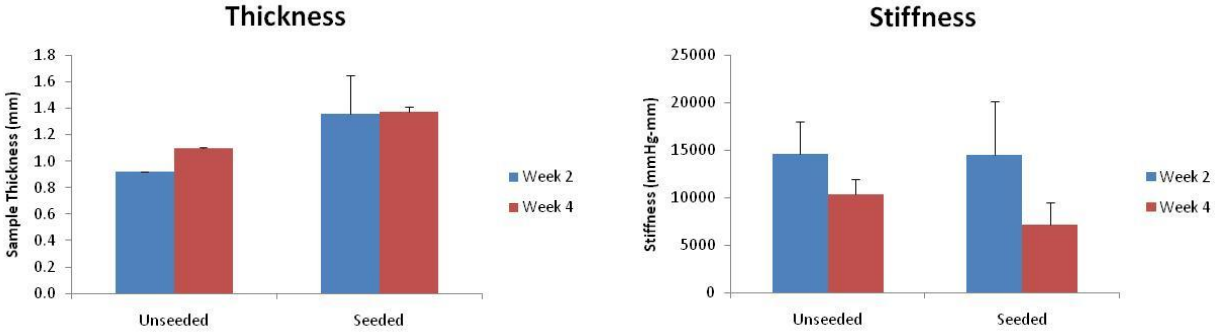

To qualitatively assess the structural changes which occurred in the scaffold during incubation, sections of control scaffolds and scaffolds cultured with fibroblasts for 4 weeks were analyzed using the orcein stain to visualize elastin. As shown in the figure below, the elastic fibers appear smaller and more frayed in the sample incubated with fibroblasts. This may be indicative of scaffold degradation.

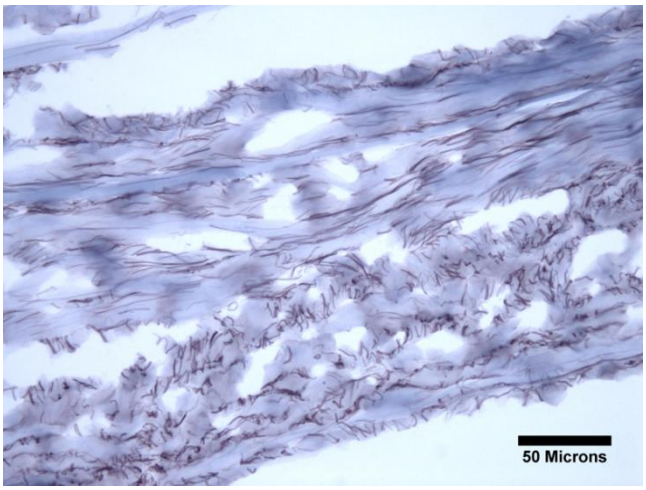

Control Veritas

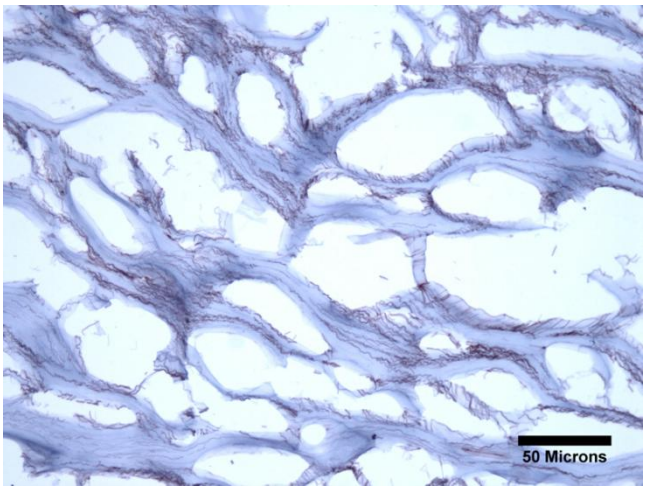

Fibroblast Seeded, 4 Weeks

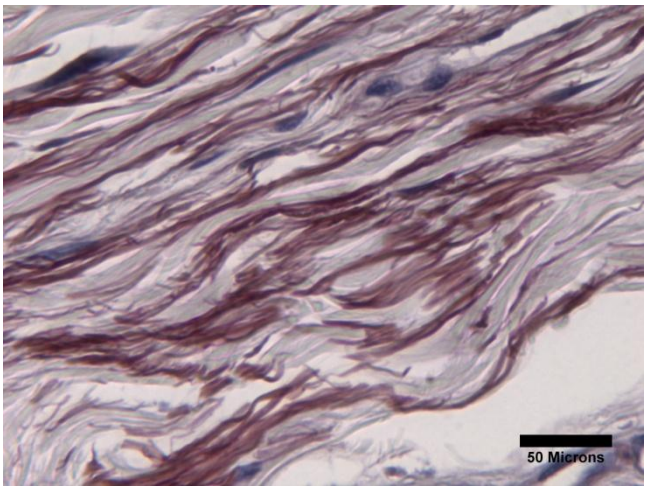

Skin Control